

We are IntechOpen, the world's leading publisher of Open Access books Built by scientists, for scientists

5,000

Open access books available

125,000

International authors and editors

140M

Downloads

Our authors are among the

154

Countries delivered to

TOP 1%

most cited scientists

12.2%

Contributors from top 500 universities



WEB OF SCIENCE™

Selection of our books indexed in the Book Citation Index
in Web of Science™ Core Collection (BKCI)

Interested in publishing with us?
Contact book.department@intechopen.com

Numbers displayed above are based on latest data collected.
For more information visit www.intechopen.com



Catalytic Micro/Nanomotors: Propulsion Mechanisms, Fabrication, Control, and Applications

Liangxing Hu, Nan Wang and Kai Tao

Abstract

Micro-/nanomotors are self-propelled micro-/nanomachines, which are capable of converting the surrounding fuels into mechanical movement or force. Inspired by naturally occurring biomolecular motor proteins, scientists extensively paid great attentions to synthetic micro-/nanomotors. Especially, a number of researchers devoted their efforts onto catalytic micro-/nanomotors. In the past few decades, several advanced developments and excellent contributions have been made in catalytic micro-/nanomotors. The future of this research field can be bright, but some major existing challenges such as biocompatible materials and fuels, smart controlling, and specifically practical applications are still required to be resolved. Therefore, it is essential for us to learn the state of the art of catalytic micro-/nanomotors. In this chapter, the propulsion mechanisms, fabrication methods, controlling strategies, and potential applications of catalytic micro-/nanomotors are presented and summarized.

Keywords: catalytic micro-/nanomotors, propulsion mechanisms, fabrication methods, controlling strategies, applications

1. Introduction

Movement is crucial for all different types of lives existing in both macroscopic and micro-/nanoscopic environments. Nature has developed smart and high-efficiency biomolecular motor proteins through such many years of biological evolution and has employed them in numerous biological processes and cellular activities [1–3]. For instance, bacteria are able to propel themselves forward with the aid of rotary flagellar nanomotors, as shown in **Figure 1A** [1]. Moreover, linear biomolecular motor proteins, such as kinesin, myosin, and dynein, are capable of harvesting energy from hydrolyzing adenosine triphosphate (ATP) into adenosine diphosphate (ADP) and phosphate (Pi) molecule for lateral motion along corresponding tracts, as shown in **Figure 1B** [2]. In addition, biological cells are equipped with intelligent biomolecular engines (ATPase), which are demanded to generate biological fuel ATP, as shown in **Figure 1C** [3].

Micro-/nanomotors are micro-/nanoscale devices, which possess the ability to convert chemical energy into mechanical force or movement [4]. Evolution bestows

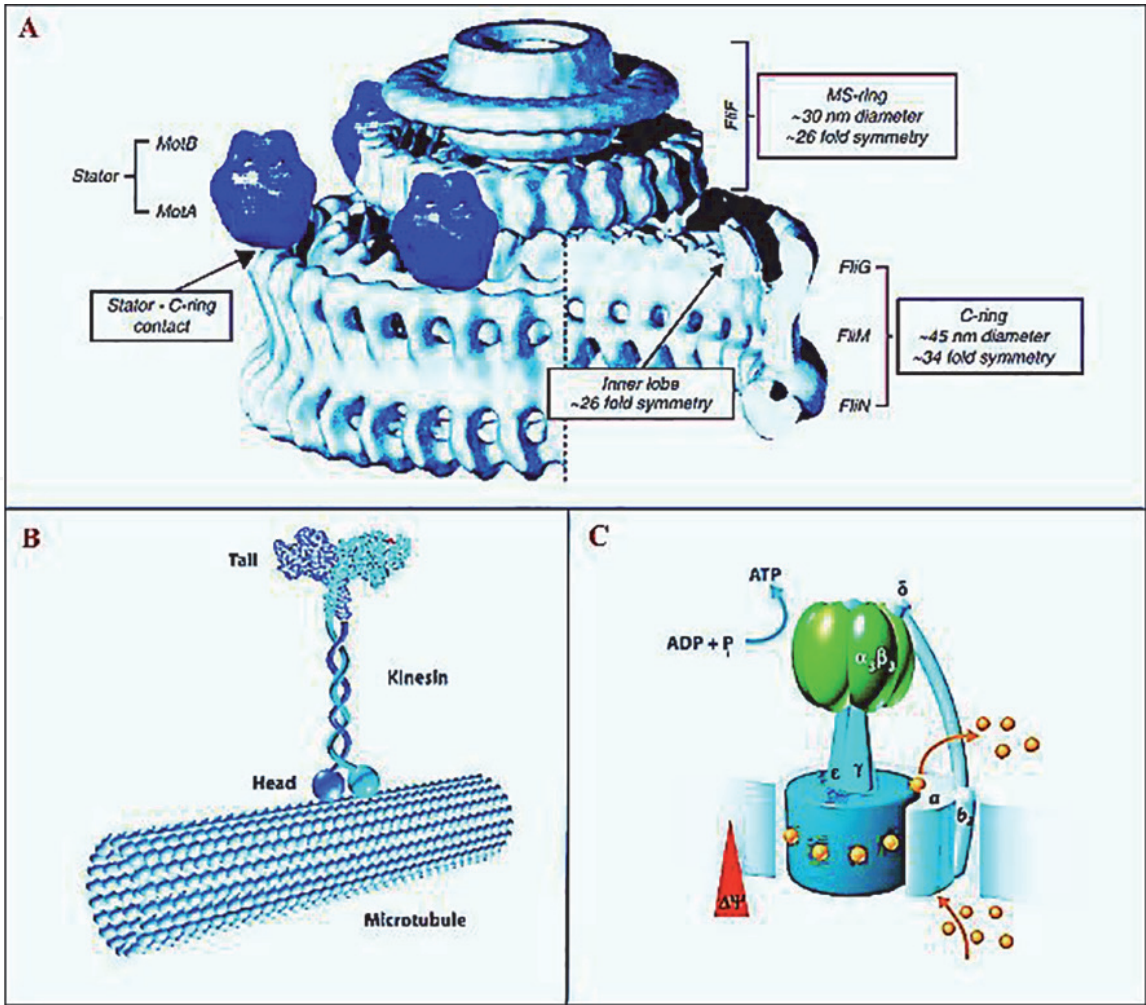


Figure 1. (A) Schematic diagram of the architecture of the bacterial flagellar motor. (B) The twin heads of kinesin motor protein alternately bind to the microtubules so that the protein motor moves forward. (C) Schematic diagram of ATPase. Copyright 2012, Elsevier. Copyright 2004, IEEE Xplore Digital Library. Copyright 2000, The Royal society Publishing.

biomolecular protein motors with fascinating abilities to harness energy from living environments for autonomous motion *in vivo* as described above. Inspired by the fantasy of naturally occurring motor proteins, researchers paid great attentions into synthetic micro-/nanomotors in the past decades. In particular, led by pioneering contributions of Sen and Mallouk’s team and Ozin’s group, current work mainly focuses on the exploration of high-efficiency and high-speed synthetic micro-/nanomotors that are able to convert chemical energy into autonomous propulsion [4–6].

The research of synthetic self-propelled micro-/nanomotors has rapidly developed in last few decades [4–9]. Several advanced developments and excellent contributions had been made in this field. Although the bright future of this research area can be expected, some major existing challenges are still remained to be solved. The design, fabrication, and characterization of functional micro-/nanomotors require some innovative approaches and ideas to realize. Fabricating micro-/nanomotors with individual functional parts, smartly and precisely controlling motors are still extremely challenging. Hereby, a complete understanding of the physiochemical mechanism is necessary. To realize better control of micro-/nanomotors in the future, an industrial level of functional micro-/nanomachinery could be achieved. Despite of the significant development and advances in micro-/nanomotors, challenges are still remained to find specific relevant applications, such as biologically compatible fuels, etc.

Meanwhile, micro-/nanomotors have a wide variety of applications, including cargo towing, water cleaning, chemical sensors, biomedical applications, etc. [5, 7–9]. Advanced forms of micro-/nanomotors may stimulate and benefit other research. However, designing and powering micro-/nanomotors can be considered as a significant challenge in today's nanotechnology research. Hence, it is much beneficial for us to learn the state of the art of synthetic micro-/nanomotors and improve them in this research field. In this chapter, the reported work on the propulsion mechanisms, fabrication methods, propulsion controlling, and applications of synthetic self-propelled platinum-based micro-/nanomotors will be presented and discussed.

2. Propulsion mechanisms

Whitesides and his colleagues firstly reported the motion of a millimeter-scale object, which was composed of a piece of platinum (Pt)-coated porous glass filter mounted on a thin polydimethylsiloxane (PDMS) plate using a stainless steel pin, as shown in **Figure 2** [10]. The assembled object was immersed into hydrogen peroxide (H_2O_2) solution. Pt catalyzes H_2O_2 decomposition to generate oxygen (O_2) bubbles releasing from its surface, which reversely induced a recoil force to propel the object moving forward. This is the foundation in this research field. In micro-/nanoscale regime, only asymmetric particles can realize autonomous propulsion. Based on this, researchers focused on two aspects: shape and material compositions of micro-/nanomotors for breaking the symmetry, and various types of micro-/nanomotors were invented. Meanwhile, there were different mechanisms proposed to explain the propulsion phenomena, depending on the shapes (e.g., wires, rods, Janus spheres, and tubular jets) and material compositions of micro-/nanomotors [4–17].

2.1 Dielectrophoresis

In the past decades, a variety of micro-/nanomotors have been envisioned to explore the concept of self-electrophoresis propulsion, especially micro-/nanowires, rods, and Janus spheres. In self-electrophoresis, micro-/nanomotors produce a locally distributed electric field through chemical gradients and propel forward in

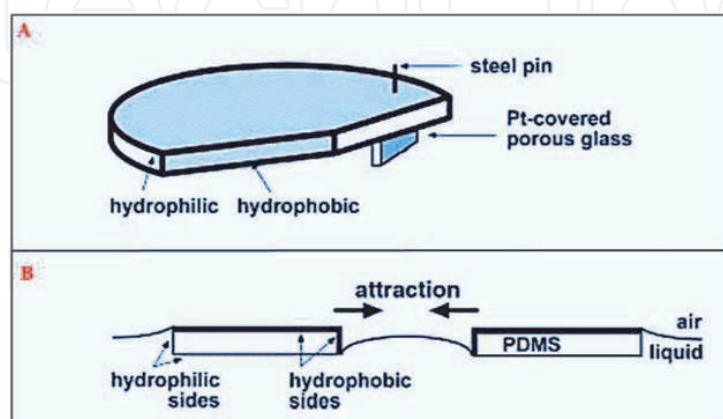


Figure 2.

(A) Schematic diagram of the propulsion of a millimeter-scale object. A thin plate (1–2 mm in thickness and 9 mm in diameter) was assembled from PDMS in a desired shape, and specified faces were rendered as hydrophilic by plasma oxidation. A $2 \times 2 \text{ mm}^2$ piece of porous glass filter (one side covered with Pt) was mounted on the PDMS plate by using a stainless steel pin. (B) A diagram illustrating self-assembly by capillary interactions. Copyright 2002, Wiley Online Library.

respond to this self-produced electric field, and they do not respond to an external electric field.

Electrophoresis describes the movement of micro-/nanoscale particles in a fluid. In dielectrophoresis, if a micro-/nanoparticle would realize autonomous self-propulsion, the micro-/nanoparticle must contain at least two different metals and acts as a self-contained electro-chemical cell. For instance, a micro-/nanorod is composed of Pt and gold (Au), Au serves as the cathode and Pt is the anode, as shown in **Figure 3** [6].

The oxidation of H_2O_2 at the Pt side (anode) of the rod generates negatively charged electrons (e^-) and positively charged protons (H^+). The generated protons migrate along the double layer surrounding the rod and the electrons internally migrate along the rod from the Pt side to the Au side (cathode) of the rod; thus, H_2O_2 can be converted into water (H_2O) and O_2 . The continuous chemical reactions result in a net flow of electrons from the anode to the cathode as well as the migration of protons to the cathode, producing a proton gradient along the axis of the rod. The electron flow produces a negatively charged rod that responds to the gradient, which propels the rod forward to the proton-rich environment previously occupied by Au [6].

In self-electrophoresis, the charged micro-/nanoparticles propel forward in a self-generated electric field resulting from an uneven distribution of ions. The velocity v of the particle is related to the self-produced electric field (E), zeta potential (ζ) of the particle, permittivity (ϵ), and viscosity (μ) of the medium, as shown below:

$$v = \frac{\zeta \epsilon E}{\mu} \quad (1)$$

2.2 Diffusiophoresis

Self-diffusiophoresis is a propulsion phenomenon in which the movement of particles is induced by a concentration gradient of the reaction products. This propulsion mechanism is more commonly employed in spherical Janus micro-/nanomotors, as shown in **Figure 4** [11, 12]. In this system, the catalyst (Pt) is located at one side of the micro-/nanomotor; the reaction products (H_2O and O_2) preferentially accumulate at the site of the catalyst. Hence, a concentration gradient

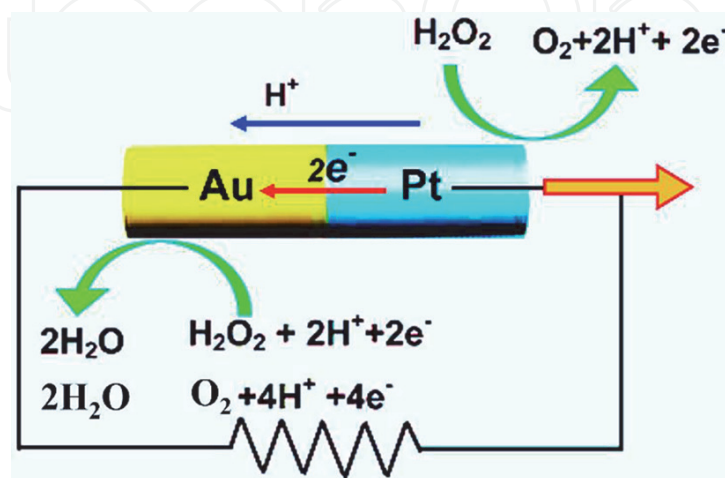


Figure 3. Schematic representation of dielectrophoresis (bipolar electrochemical) mechanism for the propulsion of an Au-Pt micro-/nanomotor in the presence of H_2O_2 . The mechanism involves an internal electron flow from one end to the other end of the motor, along with the migration of protons in the double layer surrounding the motor. Copyright 2006, ACS Publications.



Figure 4. Schematic diagram of a micro/nanomotor propelling under the diffusiophoresis propulsion mechanism. Copyright 2009, Wiley Online Library. Copyright 2011, Frontiers Journals of Higher Education Press.

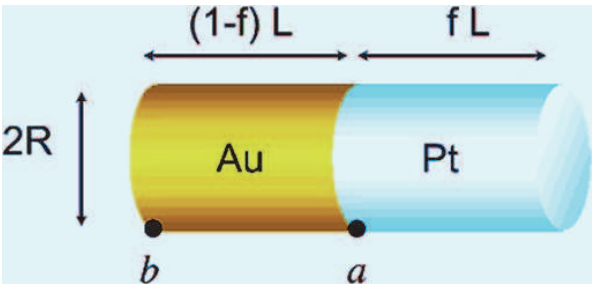


Figure 5. Schematic illustration of a Pt-Au nanorod representing the dimensions used in the calculation of interfacial force. The parameter f is the length ratio of Pt. Copyright 2004, ACS Publications.

is produced along the surface of the micro-/nanomotor. As the reaction products reach a certain point, the local concentration is higher and the products start to diffuse away from the catalyst, which in turn produces a force leading to the movement of the micro-/nanomotor.

2.3 Interfacial tension

Surface tension gradient along an interface can result in an imbalanced force and further produce flow, which is well known as the “Marangoni effect.” This motion mechanism has been employed to explain the propulsion of the micro-/nanomotors, and the model was firstly reported by Crespi, Mallouk, and Sen, as shown in **Figure 5** [13]. As H_2O_2 is decomposed at the Pt side of Au-Pt nanorods to produce H_2O and O_2 , leading to an interfacial tension created near the surface of Pt is lower due to a larger quantity of O_2 generated. The surface tension difference between the Pt side and the Au side produces a force to thrust the micro-/nanomotor propelling forward.

In this model, it is proposed that the velocity v of micro-/nanomotors is linearly proportional to the surface tension of the solution, as shown in the following equation:

$$v = \frac{SR^2\gamma}{\mu DL} \propto k\gamma \tag{2}$$

where S , R , γ , μ , D , L , and k are the O_2 evolution rate, radius of micro-/nanomotor, surface tension of solution, viscosity of solution, diffusion coefficient and length of micro-/nanomotor, and constant, respectively.

2.4 Acoustophoresis

One of the potential applications of micro-/nanomotors is to be used in diagnostics and biomedicine; there is a demand to develop propulsion mechanisms which can be biocompatible. Ultrasound operates in a range of frequency above 20 kHz, which is biocompatible [5]. Hence, ultrasound is a promising technique for propelling micro-/nanomotors (wires/rods and tubular jets) in biomedical applications. The micro-/nanomotor propelled by ultrasound was firstly reported by Sen's group in 2012, as shown in **Figure 6** [5]. In this system, metallic microrods are suspended in water surrounded by an acoustic chamber. A vertical standing wave levitates the microrods to a plane at the midpoint of the cell resulting from the lowest pressure. In that plane, the metallic microrods behave axial propulsion at speeds up to $200 \mu\text{m/s}$ in water. The microrods also assemble into patterns in the nodal plane resulting from nodes and antinodes among the plane. The composition of the microrods was observed to effectively affect their propulsion, with only metallic microparticles demonstrating fast axial motion.

2.5 Thermophoresis

Temperature gradient could introduce the motion of micro-/nanoparticles (micro-/nanowires, rods, and Janus spheres). This phenomenon is called thermophoresis or the "Soret effect." Recently, the propulsion of micro-/nanomotors induced by self-generated temperature gradient has been investigated, as shown in **Figure 7**.

Jiang et al. studied self-thermophoresis at the single particle level (**Figure 7A**) in 2010 [14]. Janus silica (SiO_2) microspheres half-coated with Au were irradiated in water by using a defocused laser beam at 1064 nm. Absorption of laser by the thin Au layer generated heat, resulting in a local temperature gradient ($\sim 2 \text{ K}$ across particles) which produced thermophoresis. After that, Baraban et al. applied an

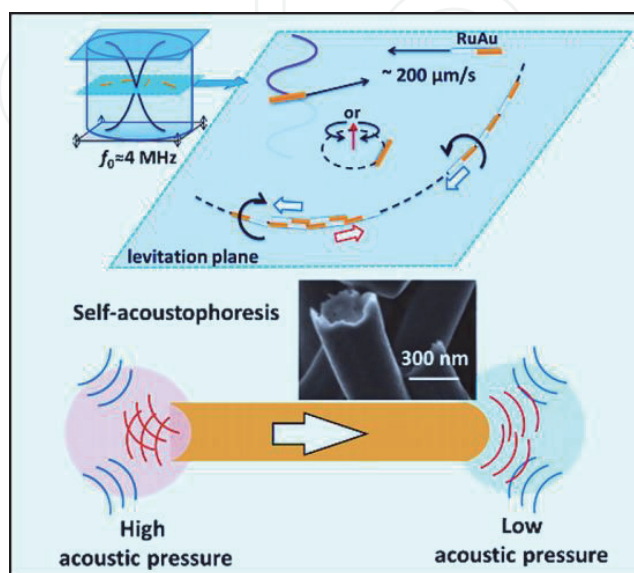


Figure 6. Self-acoustophoresis mechanism: asymmetrically shaped metallic microrods are triggered by an ultrasonic standing wave at MHz frequency. Copyright 2012, ACS Publications.

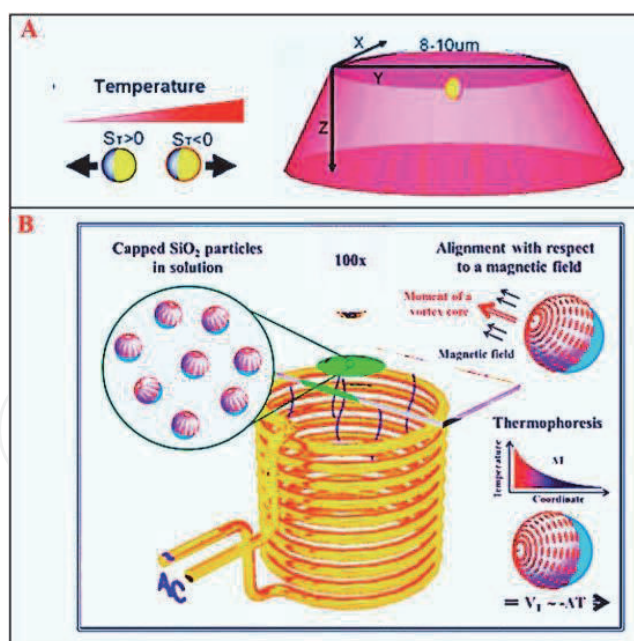


Figure 7. Self-thermophoretic microparticles. (A) Au-capped SiO_2 microspheres undergoing autonomous propulsion resulting from the “Soret effect” in a defocused laser beam. (B) Permalloy-capped SiO_2 particles moving by self-thermophoresis in an AC magnetic field. Copyright 2010, APS Publications. Copyright 2012, ACS Publications.

alternating current (AC) magnetic field to heat up and down permalloy-capped SiO_2 particles in solution and viewed autonomous movement, as shown in **Figure 7B** [15].

Short heat pulses have also been applied to modulate the speed of micro-/nanomotors. Au-Pt nanowires subjected to elevated temperatures were observed to propel forward extremely faster than those at room temperature. For instance, an average speed of $45 \mu\text{m/s}$ was obtained for nanowires at 65°C compared with $14 \mu\text{m/s}$ at 25°C . The speed increasing could be resulted from the reduction of the solution’s viscosity and the temperature dependency of the electrochemical process. The utilization of heat pulses is an extremely reversible process, after incorporated with magnetic steering, which will enable a more advanced spatial and temporal control, with the capability to modulate both the direction and the speed.

2.6 Bubble propulsion

Bubble propulsion is possibly the most commonly studied mechanism in the field of micro-/nanomotors, which can be suitable for motors with any shapes as long as the motors are decorated with catalysts. The motion of the motors is produced by the releasing of micro-sized bubbles from the decomposition of fuel catalyzed by the catalyst. The most extensively studied instances of bubble-propelled micro-/nanomotors are those decorated with Pt as a catalyst to decompose H_2O_2 into H_2O and O_2 bubbles, as shown in **Figure 8** [16, 17].

Bubble propulsion originates from the spontaneous decomposition of a fuel stimulated by a catalyst into micron-sized gas bubbles, whose detachments from the micro-/nanomotor’s surface produce a recoil force to thrust the movement of the motors in the direction away from the catalyst. These motors, whose size ranging from a few micrometers to hundreds of micrometers, can realize powerful movement with considerable speed. In bubble-propelled micro-/nanojets, Solovev and his colleagues reported that the speed of the micro-/nanojets was related to the bubble’s detachment frequency and radius, with the deviations at large values

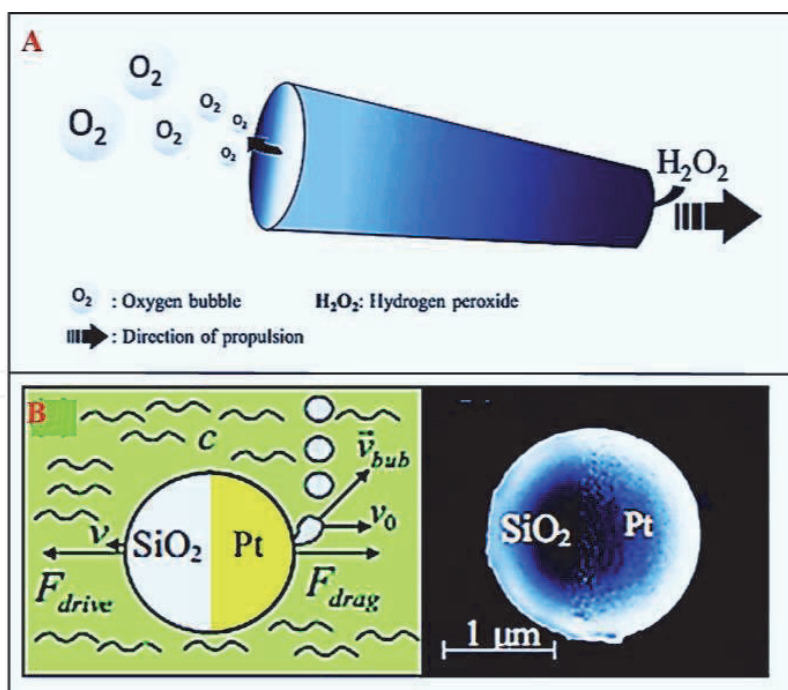


Figure 8.

Examples of bubble propelled micromotors. (A) Schematic illustration of a tubular micro-/nanomotor's movement by the bubble propulsion mechanism. (B) Janus Pt-SiO₂ spheres moving in H₂O₂. Copyright 2014, RSC Publications. Copyright 2009, AIP Publications.

resulted from the potential collisions between bubbles, which diminished the distance traveled by the bubbles within the tube and limits the detaching stage. They concluded that the dynamics of micro-/nanojets is influenced by their shapes, the fuel composition, and the viscosity of the medium.

3. Fabrication methods

Artificial micro-/nanomotors could offer a significant advance in the field of miniaturized devices. However, a major challenge in artificial micro-/nanomotor field is the synthesis of such tiny devices with high quality and reliability. Relying on the intended applications, different synthesis techniques must be taken into account, since each specifically shaped micro-/nanomotor demands a specialized synthesis technique as well as defines the desired propulsion mechanism. The rapid developing of nanotechnology has resulted in various techniques and strategies for the synthesis of micro- and nanoscale motors. The purpose of this section is to present versatile schemes to the synthesis of micro-/nanomotors. The synthesis strategies and the factors that ought to be considered in the design of micro-/nanomotors are including the shapes, compositions, and distributions of materials, and functionalization. By highlighting the progresses that have been achieved in the synthesis of artificial micro-/nanomotors over the last decades, we intend to present the challenges and opportunities facing synthesis and put forward perspectives for the upgrowth of new methods.

3.1 Electrochemical deposition

Electrochemical deposition is a process that applies external electric current to grow materials and enables the growth of arbitrary three-dimensional (3D) shapes with distinct materials varying from metals to polymers, resulting in the widespread applications of this growth strategy in nanotechnology. The process can be

conducted without the requirements of expensive instruments and harsh working environments. Therefore, micro-/nanostructures with diverse dimensions can be grown using this method, especially the micro-/nanowire, micro-/nanorod, and tubular micro-/nanoengines.

Template-assisted electrochemical deposition, as shown in **Figure 9**, utilizes the pores of a membrane template to grow the required wires and tubes comprising of different materials [18]. Each pore of the template functions as a reactor in which the desired structure is synthesized. Membrane templates commonly used for the synthesis of micro-/nanomotors are track-etched polycarbonate (PC) membranes and porous alumina (AAO) membranes. Relying on the properties of the material and the chemistry of the pore wall, the micro-/nanomotors can be either hollow or solid. Membrane template-assisted electrodeposition provides a relatively low-cost and powerful approach for synthesizing micro-/nanowires, micro-/nanorods, and tubular micro-/nanoengines.

For membrane template-assisted electrodeposition, a layer of Au or silver (Ag) is firstly coated on one side of the membrane by physical vapor deposition (PVD) to play a role of the working electrode. Afterwards, the membrane is assembled in a Teflon plating cell with flat aluminum (Al) foil located against the metal layer to work as a conductive contact for subsequent electrodeposition. Commonly, a sacrificial layer of Ag or copper (Cu) is firstly grown, followed by sequential growth of different required metals. The Ag or Au backing and the sacrificial layer are etched away by chemical etchant or are removed by mechanical polishing. By removing the alumina (Al_2O_3) membrane in sodium hydroxide (NaOH) solution, the nanowires or nanotubes can be released and obtained after successive rinsing and centrifugation.

The Wang's and Pumera's research groups combined electrodeposition widely applied in the growth of nanowire-based micro-/nanomotors with the bubble-propelled tubular micro-/nanojets, as shown in **Figure 10** [19–24]. Two geometries (either cylindrical or conical) can be obtained, entirely relying on the type and geometry of porous template (either PC or AAO). In addition to such metals, the incorporation of polyethylenedioxythiophene (PEDOT), polyaniline (PANI), and polypyrrole (PPy) polymers with Pt generates catalytic microjets. On the other hand, the wall can be incorporated with molecularly imprinted polymers (MIPs) so that alternative recognition cavities can be implemented for the selective separation of biomolecules.

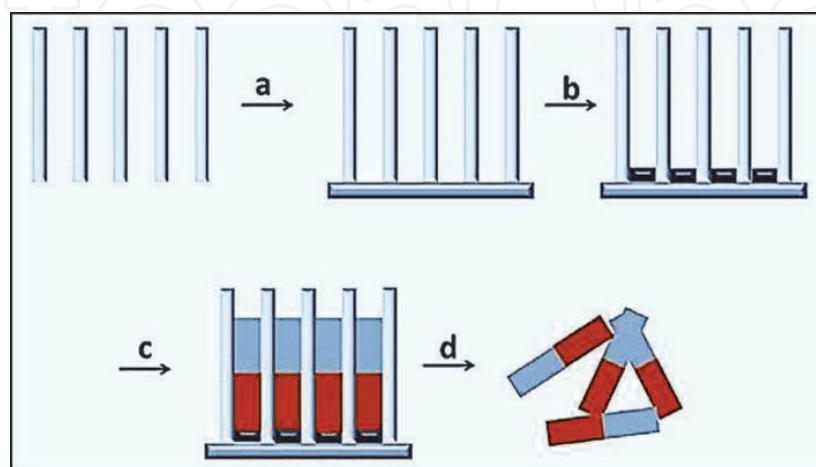


Figure 9. Membrane template-assisted electrochemical deposition of micro-/nanomotors: (a) coating of Au or Ag backing on the membrane template, (b) electrochemical deposition of the sacrificial layer, (c) sequential electrochemical deposition of desired elements, and (d) removal of the backing and sacrificial layer and dissolution of the membrane. Copyright 2015, ACS Publications.

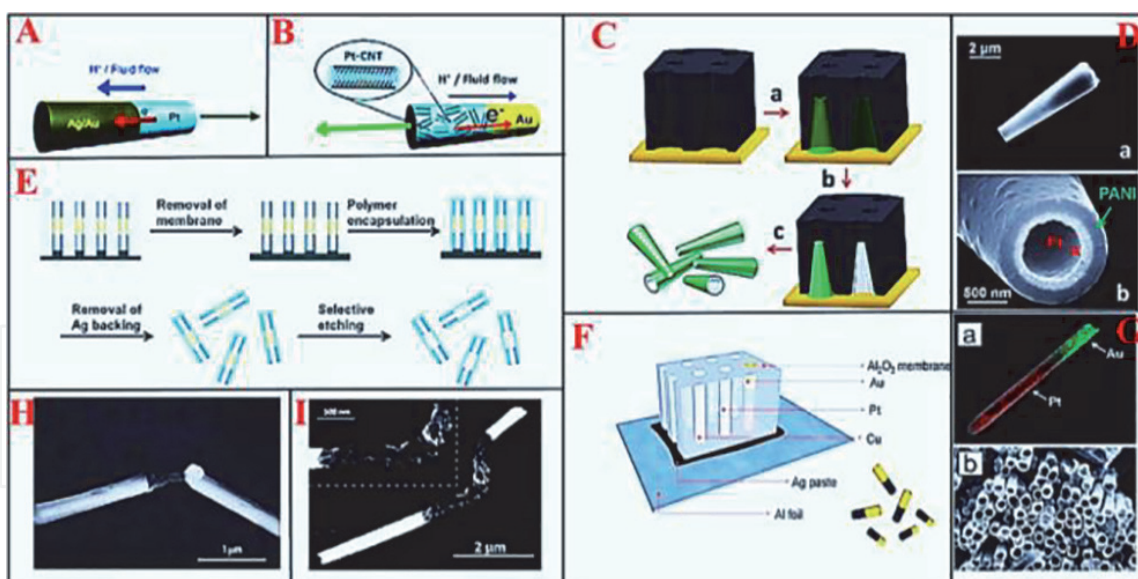


Figure 10.

Examples of micro-/nanomotors grown by template-assisted electrochemical deposition. (A) Electrodeposited Ag-Au/Pt and (B) Au/Pt-CNT nanomotors in H_2O_2 . (C, D) Polycarbonate membrane-assisted growth and SEM images of conical PANI/Pt microtubes, respectively. (E) Growth procedures of flexible metallic nanowires with polyelectrolyte hinges after membrane template electrodeposition. (F, G) Anodized AAO membrane-assisted growth and SEM (scanning electron microscopy) images of segmented microtubes, respectively. (H) SEM image of a hinged nanowire. (I) SEM image of a Au/Agflex/Ni nanomotor with flexible central Ag segment. Copyright 2008, Wiley Online Library. Copyright 2008, ACS Publications. Copyright 2011, ACS Publications. Copyright 2007, Nature Publishing Group. Copyright 2013, RSC Publications. Copyright 2010, ACS Publications.

3.2 Physical vapor deposition

PVD is a vaporization deposition process for coating thin layers of materials. The material from a solid target is firstly vaporized by a gaseous plasma or a high-temperature vacuum. Afterwards, the vapor is transferred to the surface of the substrate in vacuum or partial vacuum. Finally, it is condensed to produce thin films. The two most common kinds of PVD procedures are electron beam evaporation and sputtering. Electron beam evaporation is a process that generates an electron beam to evaporate atoms from the target into the gaseous phase, whereas sputtering creates vapor through bombardment of the target by ionized gas, typically argon (Ar). In both strategies, the produced vapor phase is subsequently condensed onto the surface of the substrate.

PVD has been shown to be an effective fabrication method in micro-/nanomotors. Compared with template-assisted electrochemical deposition, PVD has some advantages, such as the ability to coat a wide range of materials, less fabrication processes, easier to operate, and more complicated geometries of micro-/nanomotors can be fabricated. According to the deposition angles, there are two categories of PVD: conventional PVD and dynamical shadowing growth (DAG). In conventional PVD, the substrate is placed parallel to the target and the vaporized metal flux is condensed almost vertically onto the substrate. DAG or glancing angle deposition (GLAD) is a PVD strategy in which the vapor is deposited onto a substrate at an oblique angle.

Posner and co-workers reported the fabrication of a bimetallic spherical motor depending on the electrophoretic mechanism for motion, as shown in **Figure 11A** [25]. Firstly, the microspheres were half-deposited with Au by sputter machine. Afterwards, they were resuspended in water and coated again with Au in random orientation, which was repeated seven or eight times until the whole surface was fully deposited with Au. Finally, the Au-deposited spheres were half-deposited with Pt, which produced bimetallic spherical Janus micromotors that are able to propel

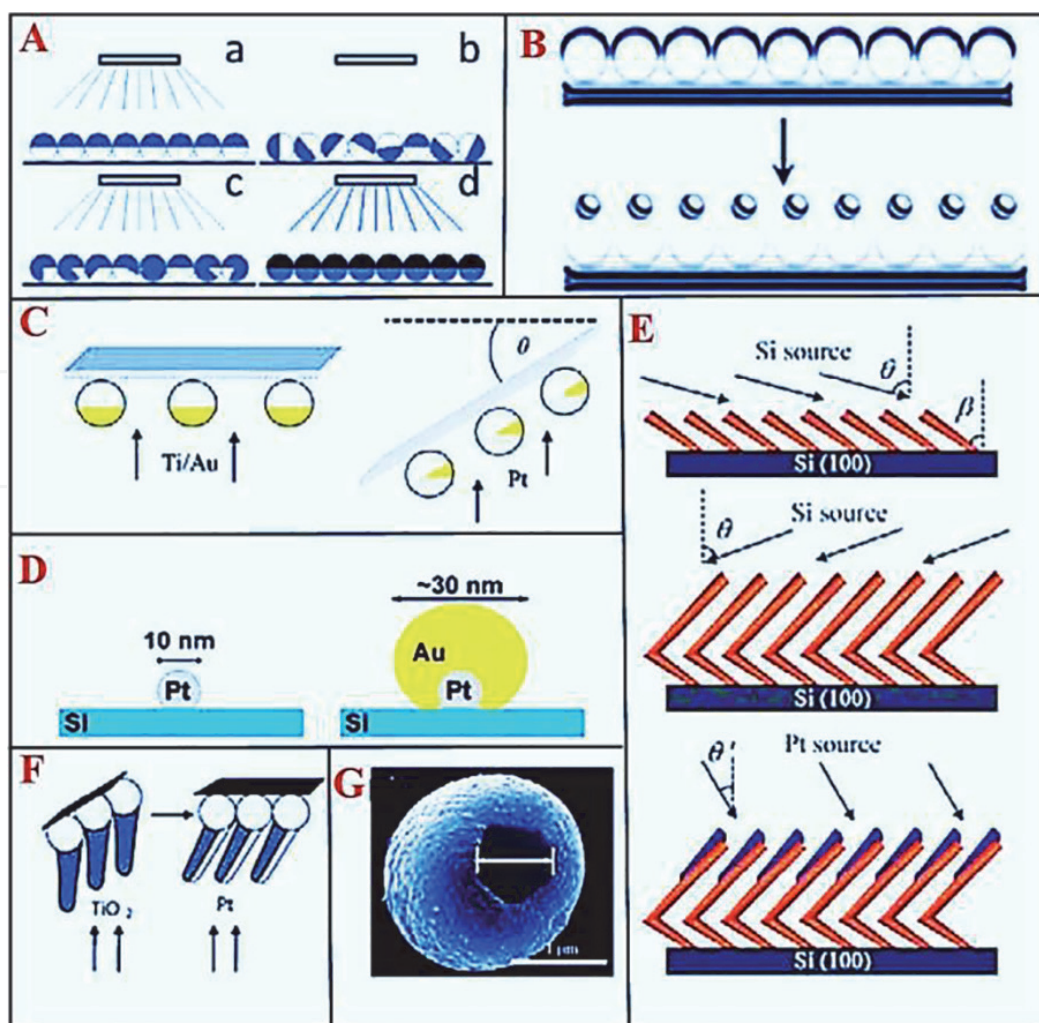


Figure 11. (A) Schematic representation of the synthesis of bimetallic Janus micromotors by conventional PVD. (B) Synthesis of sphere dimers via thermal annealing. (C) Fabrication of asymmetric Pt/Au-coated catalytic micromotors by GLAD. (D) Fabrication of electrophoretic Pt-Au Janus nanoparticles by GLAD. (E) Synthesis procedures of L-shaped Si/Pt nanorod motors by GLAD. (F) Fabrication of catalytic micromotor comprising of a spherical SiO₂ colloid with a TiO₂ arm deposited asymmetrically with Pt. (G) SEM image of a Pt-Ag-Au shell micromotor synthesized by GLAD. Copyright 2010, ACS Publications. Copyright 2010, Wiley Online Library. Copyright 2010, AIP Publications. Copyright 2014, ACS Publications. Copyright 2007, ACS Publications. Copyright 2004, ACS Publications. Copyright 2013, RSC Publications.

forward at velocities comparable to their nanowire counterparts. On the basis of sphere templates, PVD can be employed to synthesize not only spherical Janus motors but also versatile motors with various geometries. Valadares and co-workers studied a catalytic dimer comprising of a Pt half-sphere and a SiO₂ sphere. The spheres were firstly deposited with a bilayer of Cr/Pt by using sputter machine, followed by an annealing process, during which the metallic half-shell formed a Pt particle combined with the SiO₂ sphere, as shown in **Figure 11B** [26].

Relying on the substrate rotation during the deposition of an incident vapor and the self-shadowing effect, GLAD offers an easier way to synthesize Janus micro-/nanomotors with complicated geometries. Zhao and his colleagues studied the asymmetric Pt/Au-deposited catalytic micromotors synthesized by GLAD. To get an asymmetric bimetallic deposition, a SiO₂ microbeads-coated substrate was rotated to a polar angle after coating of an adhesive titanium (Ti) layer and an Au layer, the subsequent Pt coating left some of the Au layer exposed, as shown in **Figure 11C** [27]. The propulsion behavior could be regulated by changing the exposed area of the Au layer. Lee and co-workers synthesized a 30 nm Pt/Au Janus nanomotors by GLAD in which Au under fast substrate rotation was deposited onto

an array of Pt nanoparticles generated by block copolymer micelle lithography, as shown in **Figure 11D** [28]. Both of the bimetallic Janus motors depend on the self-electrophoresis mechanism for propulsion.

He and his colleagues demonstrated the synthesis of rotary silicon/Pt (Si/Pt) nanorods, Si/Ag nanorods, and L-shaped Si/Pt where they firstly applied GLAD to synthesize the Si nanorod backbone and then asymmetrically deposited a Pt or Ag layer on one side of the nanorod backbone with a geometric shadowing effect. The L-shaped backbone was fabricated by a high speed of azimuthal rotation of the substrate in the middle of oblique angle deposition, as shown in **Figure 11E** [29]. By monitoring the substrate rotation and the deposition angle, complex rolling Si/Ag springs can be synthesized. Gibbs and Zhao reported the rotary propulsion of a micromotor comprising of a SiO₂ microbead and a titanium dioxide (TiO₂) arm with asymmetric Pt deposition. The arms of the micromotors were synthesized on the closely packed microbeads at oblique angles. As such, the Pt is subsequently coated only on one side of the arms at no angle, which offers the asymmetric placement of the catalyst critical for propulsion, as shown in **Figure 11F** [13]. With substrate rotation and oblique vapor direction, the coating layer can cover a much bigger area of the sphere templates than that by using conventional vapor deposition. A bubble-propelled Pt-Ag-Au shell micromotor with a smaller opening was synthesized by GALD and subsequent wet chemical etching, as shown in **Figure 11G** [30].

3.3 Rolled-up nanotech

By combining an engineered strain gradient with the coated thin membranes, the membranes are able to roll into the required shapes when detached from the substrate. The rolled-up nanotechnology pioneered by Schmidt and co-workers applies strain engineering to form micro-/nanotubes from deposited thin films. A prestressed nanomembrane is coated onto a photoresist sacrificial layer patterned by photolithography, which is able to be alternatively etched by acetone. GLAD deposition is applied to guarantee accurate positioning and tube integration on a single chip. A proper control of the deposition rate and the substrate temperature, as well as the stress evolution during coating, creates the strain gradient desired for the rolling process.

The coated nanomembrane forms into a microtube once detached from the substrate by the dissolution of the sacrificial layer, as shown in **Figure 12A** [31, 32]. To avoid collapse of the rolled-up nanomembranes, the critical drying point is required to dry the synthesized microtubes. Microtubes with distinct opening diameters varying from 1 to 30 μm can be synthesized by modulating the built-in strain and the thickness of the nanomembranes. The lengths of the microtubes are in the range of scores of micrometers. Catalysts such as Pt consist of the inner wall of the microtubes by simply being coated onto the top layer of the nanomembranes. The wrinkle orientation of the detached membranes is defined by the different etching rates along the crystal axis and the crystal structure of the sacrificial layer.

Due to the high cost and the complex fabrication procedures of the rolled-up technique, considerable efforts have been devoted to simplifying the rolled-up procedures and decreasing its cost. Microtubes with outer layers of graphene oxide (GO) were synthesized by coating metal layers on GO nanosheets, as shown in **Figure 12B** [33]. Microscrolls with GO on the outer side and Pt at the inner surface were spontaneously synthesized upon sonication, resulting from material strain and weak bonding between GO layers. The diameter can be changed by modulating the thickness of the coated metal layers. A similar fabrication process of tubular microengines was demonstrated using accessible and low-cost fruit cells as support for the metallic layers. The tissue-based microengines can demonstrate extremely efficient bubble motion in the presence of H₂O₂. Zhao and his colleagues reported the synthesis of Pt microtubes by alternative dissolution of the poly(methyl

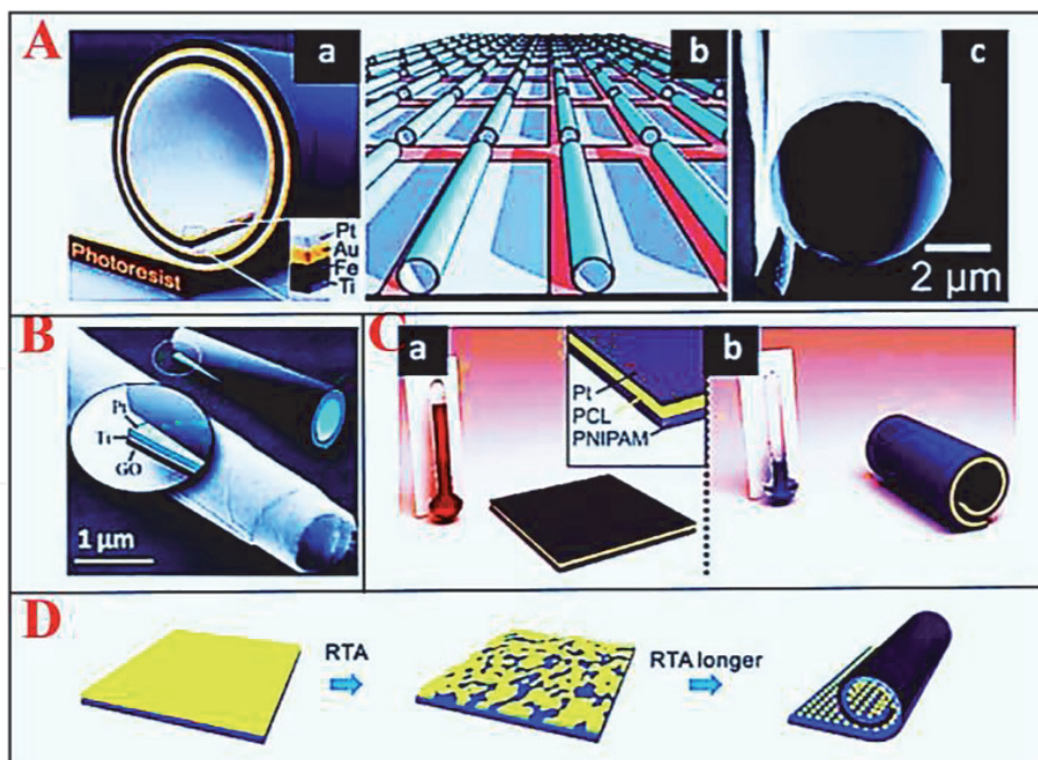


Figure 12.

Rolled-up nanotech. (A) Rolling-up of nanomembranes patterned with photoresist: (a, b) schematic illustration of a rolled-up microtube comprising of Pt/Au/Fe/Ti multilayers on a sacrificial photoresist layer and an array of rolled-up microtubes, respectively; (c) SEM image of a rolled-up microtube. (B) Rolled-up microtubes with GO as an outside layer. (C) Reversible rolling and unrolling of thermoresponsive polymeric Pt microtubes. (D) Particle-aided rolling process of nanomembrane upon a thermal dewetting treatment. Copyright 2009, Wiley Online Library. Copyright 2010, Wiley Online Library. Copyright 2012, ACS Publications. Copyright 2014, Wiley Online Library. Copyright 2013, Wiley Online Library.

methacrylate) (PMMA) sacrificial layer beneath the sputtered Pt layer or by H_2O_2 -assisted lift-off of the Pt layer coated directly on a glass wafer. A transmission electron microscopy (TEM) grid template was applied to synthesize microtubes with a relatively uniform size. Despite the low cost and simple methods described above provide great possibilities for large-scale yield of microtubes, a major issue of these methods is the lack of morphology and accurate control of the size of the rolled-up microtubes. On the premise of simplifying the processes, future efforts should be devoted to the better manipulation of the rolled-up technique.

Magdanz and his colleagues reported a flexible thermoresponsive polymeric microjet resulting from the reversible folding/unfolding of the polymer at decreased and elevated temperatures (**Figure 12C**) [34]. Cooling of the Pt/polymer layers results in folding of the films and synthesis of microtubes in diameter 30 μm with a Pt inner layer as a catalyst, while warming leads to the unfolding of the microtubes. Hence, the rolling and unrolling procedures of the microtubes could be conducted reversibly by changing the temperature of the solution to start and stop the propulsion of the microtubes. The diameters of the microtubes synthesized by the rolled-up nanotech are all in the range of microscale.

Li and his partners took advantage of the surface tension of nanodroplets as well as the intrinsic strain relaxation in the nanomembranes to reduce the diameters of the rolled-up tubes to hundreds of nanometers. A layer of Pt was coated onto a prestrained bilayer of $\text{SiO}_2/\text{TiO}_2$ or Si/Cr on a sacrificial PMMA layer, as shown in **Figure 12D** [35]. In this treatment, rapid thermal process (RTP) was applied to stretch the Pt layer to the isolated islands and the nanodroplets brought considerable surface tension for rolling. On the other hand, the removal of PMMA resulted in the detachment of the nanomembranes. The synthesized microtubes exhibit higher velocities compared with those with a smoother Pt surface.

3.4 Advanced assembling

The aforementioned fabrication methods: template-assisted electrochemical deposition, PVD, and rolled-up nanotech, are effective approaches for synthesizing micro-/nanomotors. However, to achieve more complex structures, the assembly technique must be developed. The construction of devices with multiple individual tiny parts is an extremely challenging task. The assembling approach plays an essential role in micro-/nanofabrication. It is a technique that combines miniaturized components to form a required device. The unique properties of the assembling make it applicable for the synthesis of micro-/nanomotors. Not only employing self-assembling of materials to synthesize the required devices, but also the desired elements can be embedded into micro-/nanomotors by incorporating them into materials as well.

Layer-by-layer (LbL) self-assembling is a nanofabrication strategy for multilayer formation by coating selective layers of oppositely charged materials. It is an easy-operation and low-cost process, which can encapsulate diverse materials, such as tiny inorganic compounds, colloids, macromolecules, and organic molecules together. The LbL process can be applicable for a wide range of solvent-accessible surfaces, allowing the application of different templates. Encapsulation of Pt nanoparticles enables the movement of the assembled multilayer structure to be driven in H_2O_2 solution. Taking advantages of simplicity, versatility, and low cost, the LbL assembling, primarily employing the electrostatic interaction between oppositely charged species, has been widely employed to synthesize various multilayer materials.

He's group firstly reported the combination of a colloid template-assisted LbL assembling with a microcontact printing method to synthesize platinum nanoparticles (Pt NPs) asymmetrically coated autonomous Janus micromotors, as shown in **Figure 13A** [36]. The SiO_2 particles as templates were selectively dispersed into positively charged polyallylamine hydrochloride (PAH) solution and negatively charged polystyrene sulfonate (PSS) solution to form one polyelectrolyte

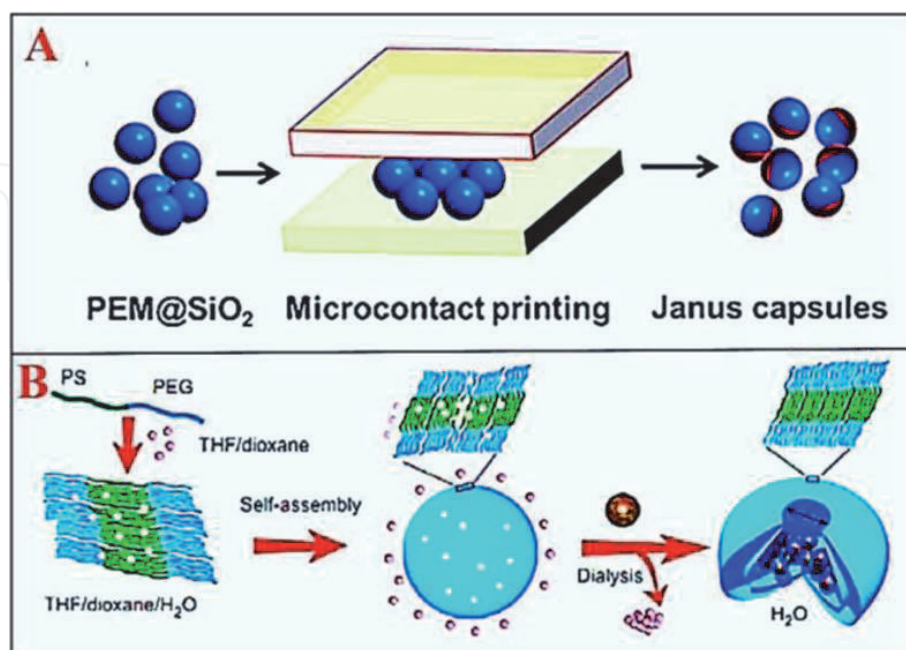


Figure 13. Schematic diagram of various types of controllable self-assembled micro-/nanomotors. (A) Synthesis process of Pt NPs-functionalized Janus capsule motors. (B) Selective and controlled encapsulation of Pt NPs inside artificial stomatocytes during shape transformation. Copyright 2012, ACS Publications. Copyright 2012, Nature Publishing group.

bilayer. After five bilayers were coated, the formed particles were spread onto a glass wafer to form a monolayer that was then printed with a PDMS stamp loaded with a drop of dendritic Pt NPs suspension. The Pt NPs partially loaded hollow Janus micromotors were collected after the removal of the templates by using hydrofluoric (HF) acid. Polymer stomatocytes that are able to entrap Pt NPs into their nanocavities were reported by Wilson and collaborators, as shown in **Figure 13B** [37]. This approach applied the controlled transformation of spherical polymersomes into stomatocyte structures. Entrapment of the Pt NPs was achieved by adding nanoparticles to solvent-swollen polymersomes during the transformation process. H_2O_2 can get in touch with the catalytic Pt NPs by controlling the entrance of the stomatocytes to produce driving force for the directional motion of the stomatocytes.

4. Controlling methods

The control of micro-/nanomotors is essential to meet various requirements in practical applications. The precise propulsion control of micro-/nanomotors is leading to advances in practical applications, and thus it is quite critical to put forward the controlling strategies for micro-/nanomotors. In the past years, scientists have realized the propulsion control of micro-/nanomotors by using different methods as reported below.

4.1 Magnetic control

External magnetic field is the most common control source employed to direct and guide the micro-/nanomotors. The predetermined trajectory of micro-/nanomotors can be realized by incorporating a paramagnetic or ferromagnetic part that can be magnetized by the magnetic field. Relying on the shapes of micro-/nanomotors, the magnetic part can be introduced by either electrodeposition or PVD. The appropriately used magnetic material candidates in micro-/nanomotors are nickel (Ni) and iron (Fe).

Wang et al. reported a multifunctional nanomotor with three segments (Au-Ni-Au), which was thrust by ultrasound and steered by the magnetic field. A concavity was also decorated at the end of the Au segment by the sphere lithography process to realize asymmetric geometry. The interaction between the magnetic field and the middle magnetic Ni segment produced a predefined and controllable movement of the nanomotor. The Ni segment was used to load and deliver magnetic particles along a predetermined route as well, as shown in **Figure 14A** [38].

Magnetic orientation has proved to be extremely effective for achieving the required directionality of the self-assembled motors. Sputtering a layer of magnetic material on one side of the motors is widely applied in Janus capsule motors. The catalase-functionalized Janus capsule motor was coated with a layer of 5-nm-thick Ni before the deposition of Au. Such biocatalytic Janus capsule motors were capable of swimming in cellular media in the presence of H_2O_2 fuel and were steered by the applied magnetic field toward the targeted HeLa cells, as shown in **Figure 14B** [39]. It should be mentioned that the magnetic field is exclusively employed to steer the propulsion directionality of motors and is not strong enough to initiate the propulsion of motors by magnetic attraction.

For electrodeposited nanowire/-rod and micro-/nanotube, a Ni part can be incorporated into the structure by using electrodeposition. A self-propelled segmented Pt/Ni/Au/Ni/Au nanowire was taken as one of the earliest examples, as shown in **Figure 14C** [40]. The nanowire was magnetized transversely rather than

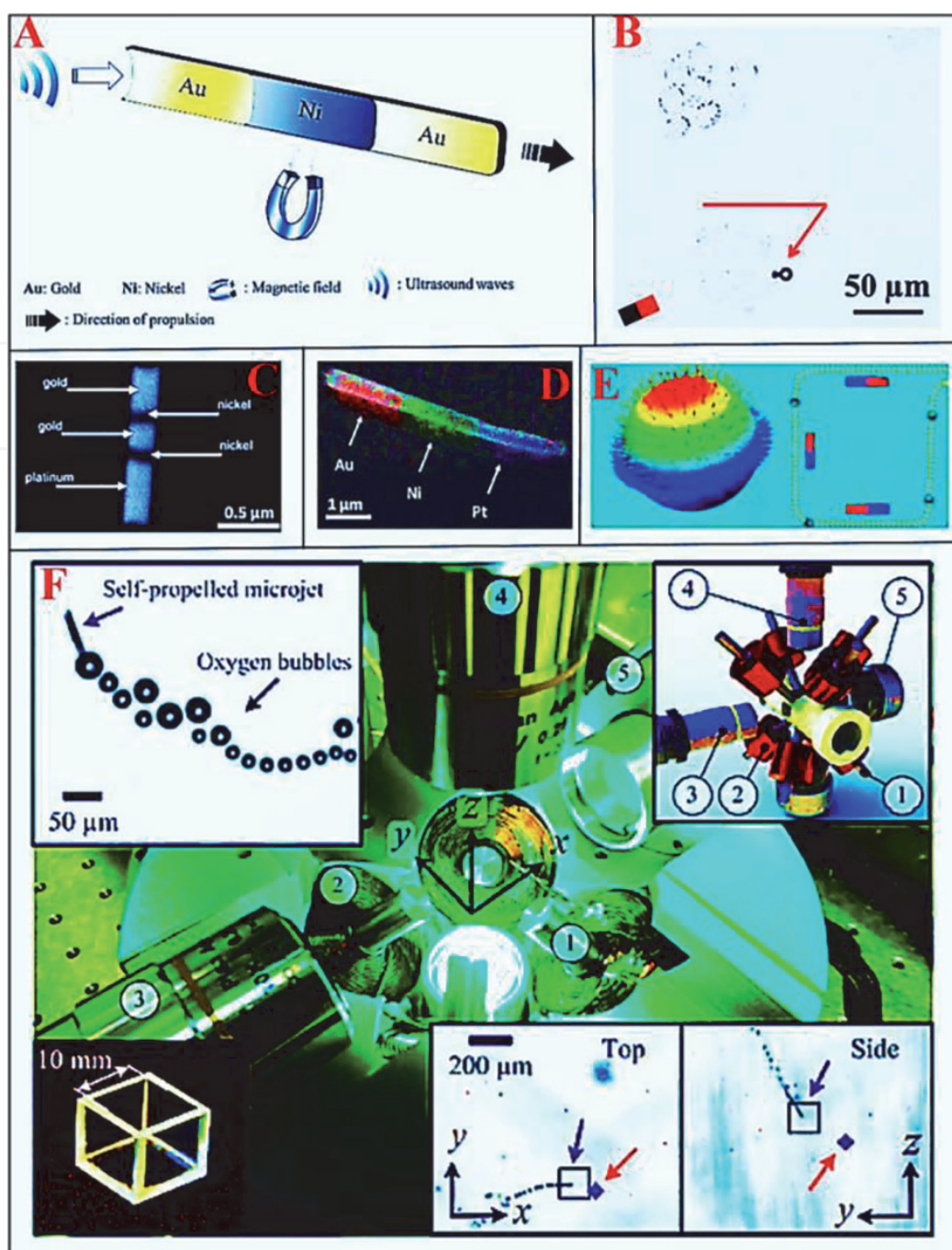


Figure 14.

Micro-/nanomotors controlled by the magnetic field. (A) Schematic diagram of an Au–Ni–Au metal alloy propelled by ultrasound and steered by the magnetic field. (B) Magnetically steered movement of Janus capsule motors toward targeted HeLa cell sheets. (C) SEM image of Pt/Ni/Au/Ni/Au nanowire. (D) SEM/energy-dispersive X-ray (EDX) elemental analysis of Au/Ni/Pt nanotube. (E) Scheme representing the magnetic steering of Janus micromotors. (F) Remote control of micro/nanojets by magnetic field. Copyright 2013, ACS Publications. Copyright 2014, ACS Publications. Copyright 2005, Wiley Online Library. Copyright 2013, ACS Publications. Copyright 2012, ACS Publications. Copyright 2013, AIP Publications.

longitudinally, resulting from the scale of the electrodeposited Ni part was smaller than the diameter of the wire. Magnetized nanowire can orient its net magnetic moment parallel to an external magnetic field, resulting in precise steering by manipulating the orientation of the magnetic field. Experimental results proved that the magnetic field could only direct the nanowires without changing their speed. The steered propulsion of self-propelled Au/Ni/Au/Pt-CNT nanorod as well as the delivery of magnetic microbead cargoes by it in microchannel networks was reported by Burdick et al. [20].

Magnetic steering of the electrodeposited microtube could also be achieved by additional electro-deposition of Ni. For conical microtube, Ni is grown to cover the

whole inner surface of the microtube before electrodeposition of Pt, resulting in the microtube is magnetized along the tube axis. A simplified Ni/Pt alloy inner layer obtained by the co-deposition of a Ni/Pt layer can display both magnetic and catalytic properties. Unfortunately, the speed of microtube with a simplified Ni/Pt alloy inner layer in diluted H_2O_2 is hugely decreased because of the reduced catalytic area. For striped nanotube with different elements placed longitudinally, it can also be magnetized longitudinally due to the Ni portion has a larger dimension along the axis of the tube, demonstrating behavior similar to that of magnetotactic bacteria, as shown in **Figure 14D** [41].

Regarding rolled-up microtube, an additional Fe layer can be integrated into the microtube during the deposition process to realize the magnetic control. The longitudinally magnetized rolled-up microtube can monitor the direction of an external field and orient itself accordingly. A magnetized Fe-contained microtube was studied to be able to selectively pick up and deliver paramagnetic beads in the absence of an external magnetic field. The ability of a Pt Janus particle to deliver cargo has been reported by Sanchez and fellows. To realize the better control of the propulsion of catalytic Janus motors and the cargo delivery process, magnetic caps consisting of (Co/Pt) multilayers were incorporated into the structure by PVD. The magnetic caps were envisioned to align the magnetic moment along the main symmetric axis of the cap, enabling direct manipulation of the Janus motor as well as superparamagnetic cargoes delivery by using an external magnetic field, as shown in **Figure 14E** [42]. Precise control of magnetic Janus particles is further reported by sorting beads between the channels in microchip devices.

The individual control of microjet in a closed-loop manner and 3D propulsion control were the next steps to be considered. Recently, Misra's and Sanchez's research groups presented the accurately closed-loop control of microjet [43]. The authors reported precisely point-to-point closed-loop control by applying weak magnetic fields (2 mT). Another study demonstrated precise control when a flow was employed against and along the propulsion direction of the microjet. An electromagnetic setup consisting of two sets of orthogonal arrays of electromagnetic coils with a Fe core in conjunction with two microscopic systems was employed to guide the movement of microjet in 3D space, as shown in **Figure 14F** [43]. Microjet overcomes vertical forces, such as vertical flow buoyancy forces, and interaction forces with O_2 bubbles, and thus it is able to drive downwards and swim upwards relative to reference positions.

4.2 Acoustic control

Ultrasound not only provides energy for the motion of micro-/nanomotors but also offers an alternative manner for controlling self-propelled motors. Using ultrasound to guide micro-/nanomotors and as rapid "stop/go" switching of micro-/nanomotors in respond to "on/off" of ultrasound are investigated.

The movement direction of nanomotors can be reversed by varying the power of the ultrasound field. Fast and reversible transitions between aggregated and free-moving states of nanomotors in H_2O_2 were obtained in response to switching between on and off ultrasound states, as shown in **Figure 15A** [44]. The generation of bubbles can be disrupted by the ultrasound field. Wang et al. demonstrated the reversible control of the propulsion of PEDOT/Ni/Pt microengines by changing the applied voltage of the external transducer which produces the ultrasound field. The authors demonstrated extremely fast changes (< 0.1 s) in the motor speed and reproducible "on/off" activations that were faster than those by using other reported methods for stopping the propulsion of microjets, as shown in **Figure 15B** [45].

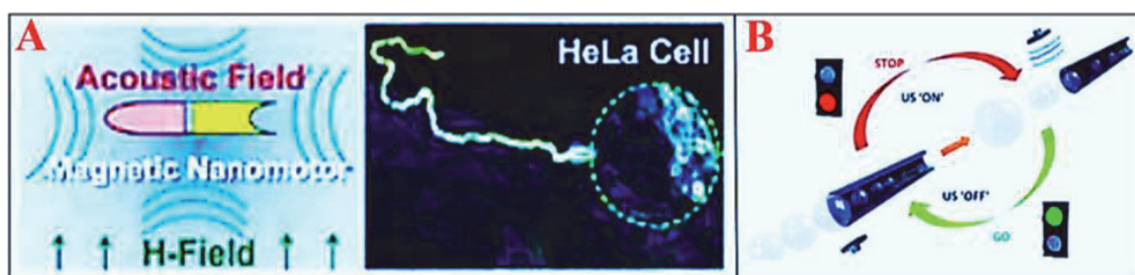


Figure 15.

(A) Scheme representing controlling of acoustically propelled nanowire toward a HeLa cell. (B) Scheme representing ultrasound-modulated bubble propulsion of chemically powered microtubes. Copyright 2013, ACS Publications. Copyright 2014, ACS Publications.

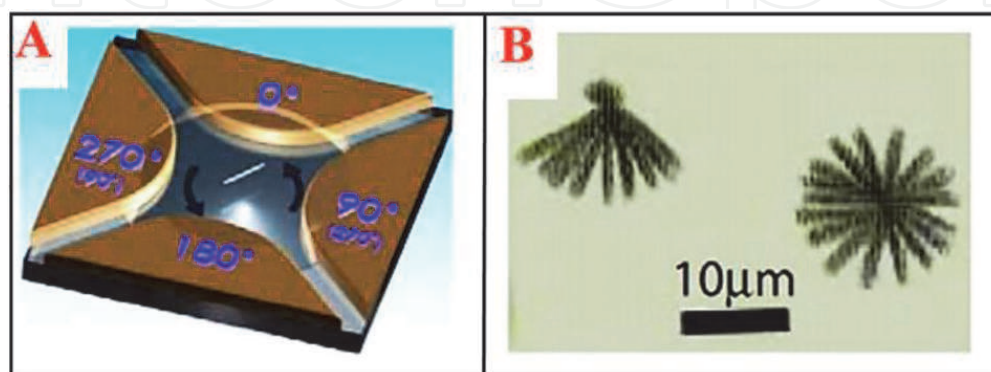


Figure 16.

Rotation of micro/nanomotors by applying AC voltages to multiple electrodes: (A) schematic diagram of experimental setup of quadruple electrodes and (B) images of one end fixed (left) and free (right) rotating Au nanowires, respectively. Copyright 2005, APS Publications.

4.3 Electric control

Metallic micro-/nanomotors can perform controllable rotation resulting from rotational torque in an electric field provided by applying AC voltages to multiple electrodes, as shown in **Figure 16A** [46]. In addition, by applying AC electric fields to strategically designed microelectrodes, the propulsion of metallic micro-/nanomotors could be tuned by dielectrophoretic force. They could be driven to chain, accelerate and align in certain directions, as well as to disperse, concentrate and assemble into complex scaffolds, as shown in **Figure 16B**.

4.4 Light control

Using the light to guide the movement of micro-/nanomotors was also reported. For example, Solovev and collaborators studied the control of microjets by using a white light source, as shown in **Figure 17A** [47]. This process was mediated through the illumination of the fuel solution above Pt-patterned Si surfaces, which generates a local decrease of the surfactant and H_2O_2 concentration. Although white light could be applied to switch off the motion of the microjets, shorter wavelengths were attributed to suppress the production of microbubbles faster than longer wavelengths. The phenomenon can be reversible, and thus a nonactive microjet is triggered by dimming the light source. Nevertheless, the “on/off” process is not immediate since it demands a few seconds to completely terminate or to reach a constantly maximum speed.

He and his colleagues recently reported the near infrared (NIR) light-switching “on/off” propulsion of Au nanoshell-functionalized polymer multilayer rockets, as

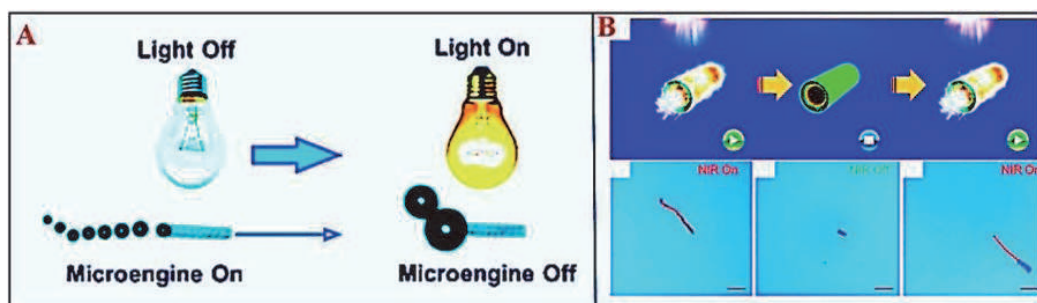


Figure 17.
 (A) Microengine's propulsion controlled by light. (B) NIR light-switchable motion of NIR propelled polymer multilayer rockets. Copyright 2011, Wiley Online Library. Copyright 2010, Wiley Online Library.

shown in **Figure 17B** [48]. NIR light irradiation could rapidly generate a thermal gradient that enables reversible movement of the Au nanoshell-functionalized polymer multilayer rockets. The rockets exhibit “on/off/on” cycles in response to an adjustable NIR irradiation, along with “go/stop/go” motions. The directional movements of the rockets were terminated as the NIR irradiation is “off” and were resumed upon switching on the NIR light. Accounting for the straight propulsion behavior of NIR-propelled polymer multilayer rockets, the “on/off” NIR switching realizes the precisely predefined route of the polymer multilayer rockets. In addition, the rockets were sustained with negligible damage under 30 times of NIR irradiation and were highly durable.

4.5 Thermal control

Thermal control of the propulsion of artificial micro-/nanomotors has proved to be applicable for both micro-/nanowires and microtubes. The speed of Pt-Au nanowires was substantially increased upon exposure to elevated temperatures. Similar phenomenon was discovered for bubble-propelled microtubes, which has been used to compensate the effect of decreasing the fuel level.

The temperature of the solution could be controlled by two Peltier elements in connection with a direct current (DC) power supply placed below the sample containing microjets. By heating up the system to a physiological temperature, microjets increase their efficiency and are propelled at extremely low concentrations of H_2O_2 , as shown in **Figure 18** [49, 50]. In addition, soft micromotors consisted of flexible thermo-responsive polymeric microjets could reversibly fold and unfold in an accurate manner resulted from the temperature change of the solution in which they are dispersed, thereby allowing them to rapidly initiate and terminate multiple times in response to the radius of curvature accordingly. The employment of stimuli-responsive materials would be ideal for the future designs of smart micro-/nanomotors.

4.6 Chemical control

The propulsion of self-propelled micro-/nanomotors could be adjusted by tuning the fuel level or chemical stimuli. In the presence of fuel concentration gradient, micro-/nanomotors can drive themselves along the gradient toward a region with a higher fuel concentration. As such, monitoring the fuel concentration and distribution can be used to direct and modulate the propulsion of micro-/nanomotors. In addition to fuel concentration, the propulsion of micro-/nanomotors is influenced by the presence of certain other chemicals. For instance, the movement of Au/Pt nanomotors was reported to be extremely accelerated upon the addition of Ag ion because of the under-potential deposition of Ag on the nanomotors, which

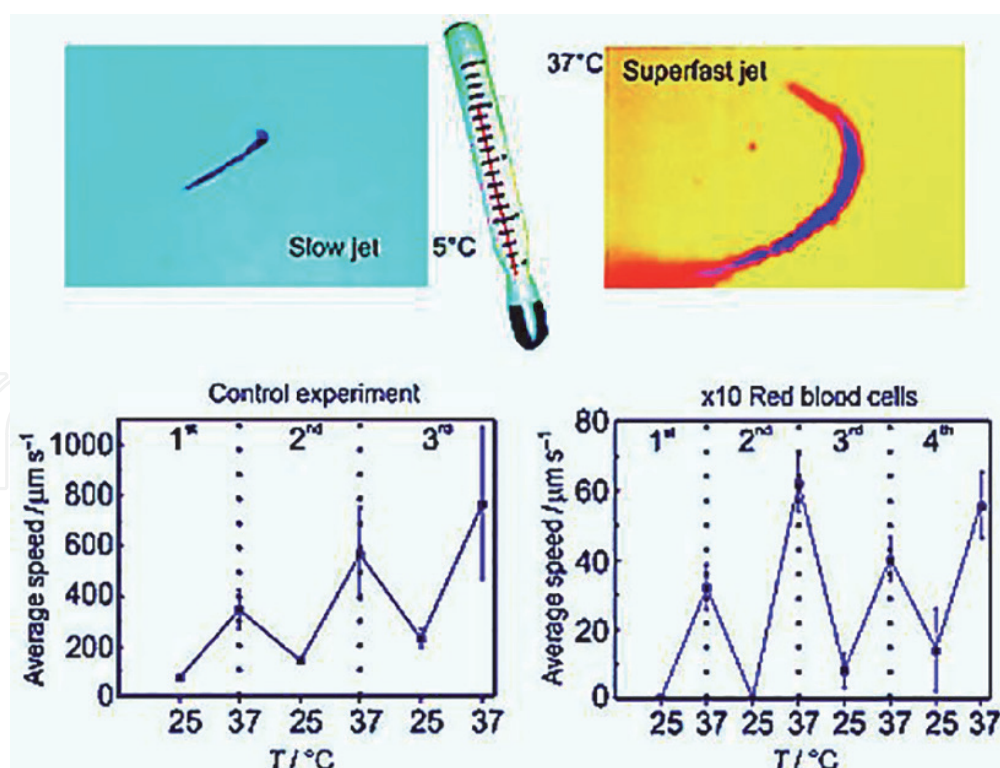


Figure 18.

Micro/nanojet's propulsion controlled by temperature. Copyright 2011, ACS Publications. Copyright 2013, RSC Publications.

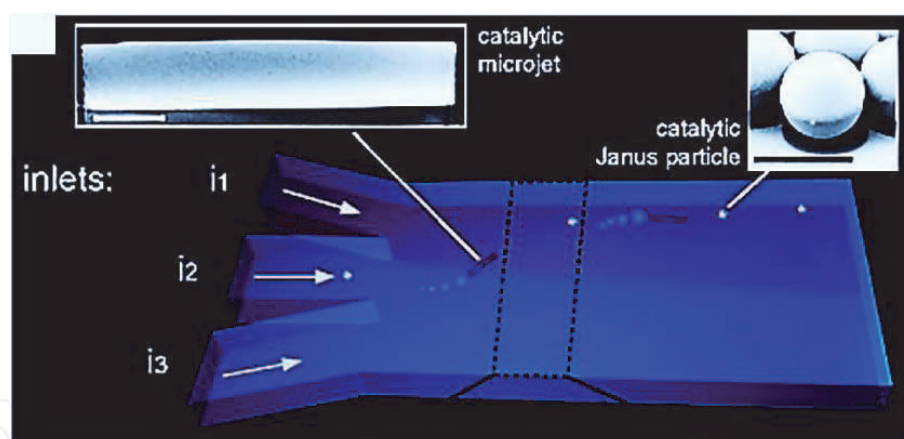


Figure 19.

Micro/nanomotor's motion controlled by chemical gradient in microfluidic channel. Copyright 2013, Wiley Online Library.

introduces differences in surface and catalytic properties. Hydrazine (N_2H_4) is another chemical stimulus observed to be effective to accelerate the propulsion of Au/Pt-CNT nanomotors. For bubble-propelled micro-/nanomotors, surfactants are significantly critical to the mobility of motors, resulting from they can stimulate bubble production and detachment.

Solovev et al. reported that the production of large microbubbles from small ensembles of microjets generated a chemophoretic attraction force and a capillary force that pulled other microjets into the swarm. A more complicated experiment was demonstrated by Baraban et al., who reported a controllable manner to study the chemotactic behavior of Janus motors and tubular microjets in microfluidic channels. Both types of motors move toward the gradient of the fuel without the influence of capillary forces, as shown in **Figure 19** [51].

5. Applications

There are many current and potential applications, resulting from the great advances in cargo-towing force, propulsion control, and lifetime of synthetic micro-/nanomotors. The wide range of potential applications of micro-/nanomotors covering different fields requires specific functionalization strategies in each kind of application. Herein, the functionalization of micro-/nanomotors for four main categories of applications is reported as follows: cargo delivery, environmental remediation, chemical sensors, and biomedical applications.

5.1 Cargo delivery

Cargo delivery is one of the most important envisioned applications of micro-/nanomotors. Relying on the properties of cargoes, tailored methods are desired for their corresponding delivery. A general process of how to synthesize micro-/nanomotors and employ them to deliver cargo molecules has been shown in **Figure 20** [4].

For the cargo delivery by micro-/nanomotors, the cargo could simply be connected to the motors by magnetic attraction. The delivery of drug-loaded magnetic poly(D,L-lactic-co-glycolic acid) (PLGA) microparticles has been studied by both chemically propelled, as shown in **Figure 21A** [52–54], and magnetically driven micro-/nanomotors. For charged cargoes, electrostatic interaction between cargoes and micro-/nanomotors could be applied for the pick-up process. A common scheme introducing charged portions into micro-/nanomotors is to incorporate a negatively charged polymer part. Sen et al. reported that a PPy part was incorporated to a nanowire via electropolymerization, which could be attached to oppositely charged polystyrene amidine cargo via electrostatic interaction, as shown in **Figure 21A**. A photo-chemically triggered cargo unloading manner was proposed for cargoes loaded nanowires via electrostatic interaction. An additional Ag portion

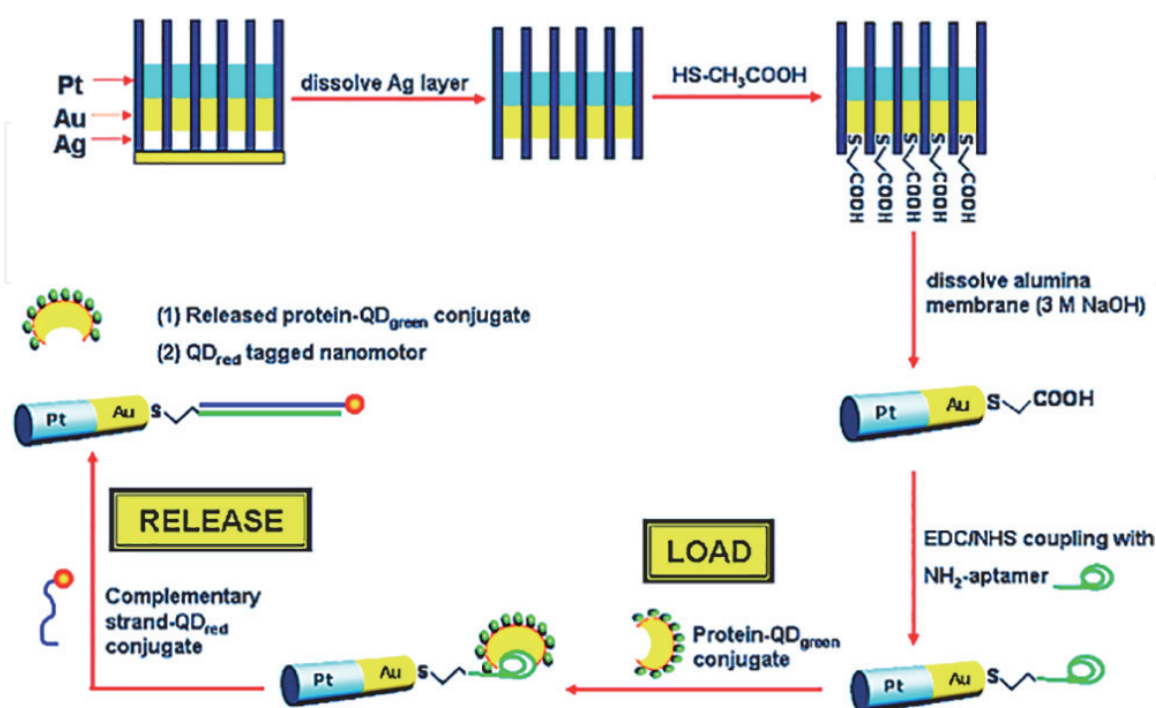


Figure 20. Electrodeposited aptamer-functionalized micro/nanomotors for selective loading, deliver, and unloading of a protein cargo. Copyright 2009, ACS Publications.

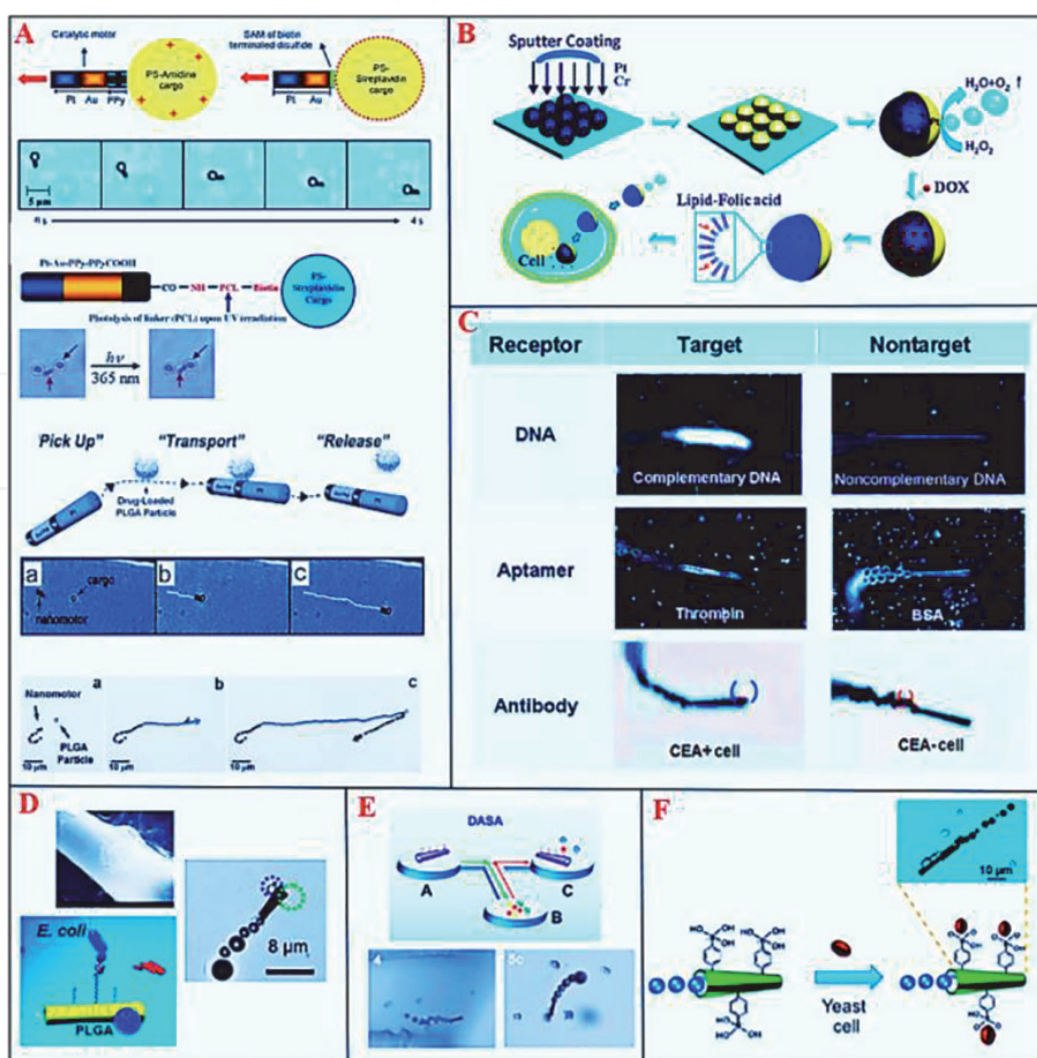


Figure 21.

(A) Examples of the delivery of cargo using solid micro/nanorods: (a) cargo pick-up, (b) cargo delivery, and (c) cargo release, respectively. (B) Synthesis procedures for Janus spherical micro/nanomotors, drug picking-up, lipid bilayer functionalization, and drug unloading (DOX = doxorubicin hydrochloride). (C) Selective binding and delivery of biological analytes and cells by functionalized microjets. (D) Direct optical visualization of pick-up, transportation, and delivery of *E. coli* bacteria and polymeric drug-carrier spheres. (E) In-chip immunoassays for in situ picking up and delivery of target proteins. (F) Selective recognition of monosaccharides for loading and unloading of yeast cells. Copyright 2008, ACS Publications. Copyright 2010, Wiley Online Library. Copyright 2010, Wiley Online Library. Copyright 2014, Wiley Online Library. Copyright 2011, RSC Publications. Copyright 2012, ACS Publications. Copyright 2013, RSC Publications. Copyright 2012, ACS Publications.

in a nanowire will be dissolved rapidly in the presence of H_2O_2 , chloride ions (Cl^-), and ultraviolet (UV) light, resulting in releasing of the cargo.

Garcia-Gradilla and colleagues demonstrated that the incorporation of a negatively charged polypyrrole polystyrene sulfonate (PPyPSS) portion with an ultrasound-propelled nanowire could be served as a pH-sensitive carrier for positively charged drugs via electrostatic interaction. The unloading of the drugs was theoretically realized by a protonated PPyPSS portion in an acidic environment. The same group also reported drug-loaded nanowires depending on a nanoporous Au portion with a large surface area. Such a nanoporous device is synthesized by dealloying the Ag portion of an Au/Ag alloy grown by the coelectrodeposition of Au and Ag. The picking up of the drug doxorubicin in the nanopores via electrostatic interactions with the polymeric coating of the nanowire motors and NIR light-stimulated drop off were reported as well.

Xuan et al. reported the fabrication of self-propelled Janus nanomotors in a diameter of 75 nm. The steps are illustrated in **Figure 21B** [55]. Spherical

mesoporous SiO₂ nanoparticles (MSNs) were fabricated by using a base-catalyzed sol-gel method. Afterwards, MSNs were dispersed on an Si substrate to form a monolayer and subsequently deposited with evaporated Cr (chromium) and Pt. A brief sonication resulted in the Janus MSNs becoming spread in a solution of the anticancer drug doxorubicin hydrochloride to pick up the cargo, and subsequently mixing with 1-mg mL⁻¹ egg phosphatidylcholine containing 1% folic acid resulted in encapsulation.

The Wang's group reported a great capability of microtubular motors for the selective loading, delivery, and isolation of distinct target analytes of biological relevance. They bio-functionalized the outer walls of microtubes with antibodies, aptamers, lectin receptors, and ss-DNA, and thus the isolation modes of cancer cells, bacteria, proteins, and nucleic acids could be demonstrated in **Figure 21C** [56]. The authors made use of rolled-up microtubes with Au layers for thiol modification and template-assisted microjets with polymer walls.

Campuzano and his colleagues functionalized Au/Ni/PANI/Pt micromotors with concanavalin A (ConA) to enable selective loading of pathogenic bacteria from fuel-enhanced real samples, as shown in **Figure 21D** [57]. The loading, transport, and unloading events were observed by optical microscopy. The delivery of pathogenic bacteria by magnetic polymeric drug carriers could represent the basis of an attractive propulsion-based theranostics scheme. In related work, the same group later functionalized artificial catalytic micromotors with antibodies to enable in-chip immunoassays, as shown in **Figure 21E** [58]. Kuralay et al. fabricated poly(3-aminophenylboronic acid) (PAPBA)/Ni/Pt tubular micromotors that selectively recognize monosaccharides, which were capable of loading and drop off of yeast cells, as shown in **Figure 21F** [59].

5.2 Environmental remediation

One of the primary environmental applications of micro-/nanomotors is to adsorb the pollutants in water. Remediation agents could be incorporated with micro-/nanomotors as the outer surface to contribute to the purification process during propulsion. Soler et al. studied the application of microtube motors decorated with a Fe outer surface to degrade organic contaminants in water via the Fenton oxidation, as shown in **Figure 22A** [60]. Wang et al. reported the application of PEDOT/Pt microtubular motors to promote the degradation of chemical threats, as shown in **Figure 22B** [61]. In brief, the oxidation of an organophosphate nerve agent by H₂O₂ was enhanced in the presence of the self-propelled micromotors, which resulted in an efficient mixing of the treated aqueous solution without the aid of external mechanical stirrers.

Surface modifications of micro-/nanomotors with a hydrophobic layer could also activate them to load oil droplets. Guix et al. demonstrated that the functionalized Au/Ni/PEDOT/Pt microtubes with a self-assembled monolayer (SAM) of alkanethiols on the Au outer surface could pick up and deliver oil droplets resulting from strong interactions between them, as shown in **Figure 22C** [62]. The same group also incorporated the rough external Au layer of microengines with long chains of self-assembled monolayers to create a super-hydrophobic absorbent layer for oil loading, as shown in **Figure 22D** [62].

5.3 Chemical sensors

The application of micro-/nanomotors as chemical sensors is based on the case that the propulsion speed of micro-/nanomotors can be converted into an analytically useful signal. The interaction of certain compounds in the sample with the

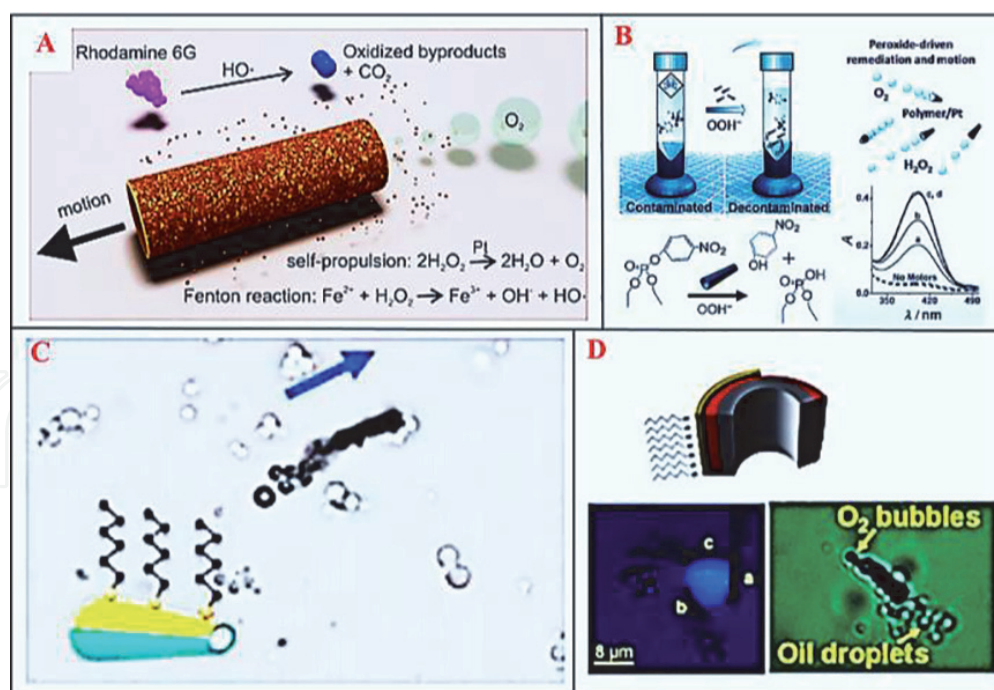


Figure 22.

(A) Organic pollutants degraded by multifunctional Fe/Pt micromotors in H_2O_2 solutions. (B) Accelerated oxidation of organophosphate nerve agents by using micromotors as active mixers. (C) Loading of oil droplets by alkanethiol-modified microtubes. (D) Picking up and loading of oil, enabled by a superhydrophobic-modified outer layer. Copyright 2013, ACS Publications. Copyright 2013, Wiley Online Library. Copyright 2012, ACS Publications.

catalytic sites of micro-/nanomotors leads to the alteration of their propulsion speed and is related to the concentration of an analyte in solution, as shown in **Figure 23** [63–66]. Although the field is still in its infancy, micro-/nanomotors as chemical sensors could have a number of advantages over conventional either optical or electrochemical sensors, such as sensitivity, selectivity, immunity to electrical interferences, operation in a wireless manner, and only requiring a minute amount of sample. In the past few years, some research groups demonstrated the ability of micro-/nanomotors to detect inorganic electrolytes present in blood, heavy metals, organic compounds such as dimethyl sulfoxide (**Figure 23A**) [63], uric acid, blood proteins such as bovine serum albumin (BSA), glucose oxidase enzymes and g-globulin, amino acids containing thiol groups, for instance, methionine, cysteine, and serine (**Figure 23D**) [65], peptides such as glutathione, and DNA (**Figure 23A**).

García and his colleagues demonstrated the first antibody-loaded tubular microengines, which were developed to load and deliver target molecules between different microfluidic chambers. Catalytic polymer/Ni/Pt microengines were bio-functionalized with antibodies targeting Immunoglobulin G (IgG) protein molecule, as a model protein, in order to realize a micromotor-based immunoassay providing “on-the-fly” loading and isolation/sorting capabilities, as shown in **Figure 23B** [57]. The immunocomplex could be simply observed by optical microscope through using an antigen/antibody labeled with a polymeric sphere tracer. This innovative work is highly selective and excludes time-consuming washing steps, accelerating and simplifying the general immunoassay procedures. Taking advantage of these features, Yu et al. employed antibody-loaded AuNP/PANI/Pt micromotors to exhibit rapid “on-the-fly” sandwich immunocomplexes targeting carcinoembryonic antigen. The operation takes 5 minutes with a measuring threshold of $1\text{--}1000\text{ ng mL}^{-1}$. In addition, labeling the loaded proteins with microscopic particles demonstrating different sizes and shapes facilitates the multiplexed analysis of proteins, as proved by Vilela and his colleagues (**Figure 23C**) [64]. In

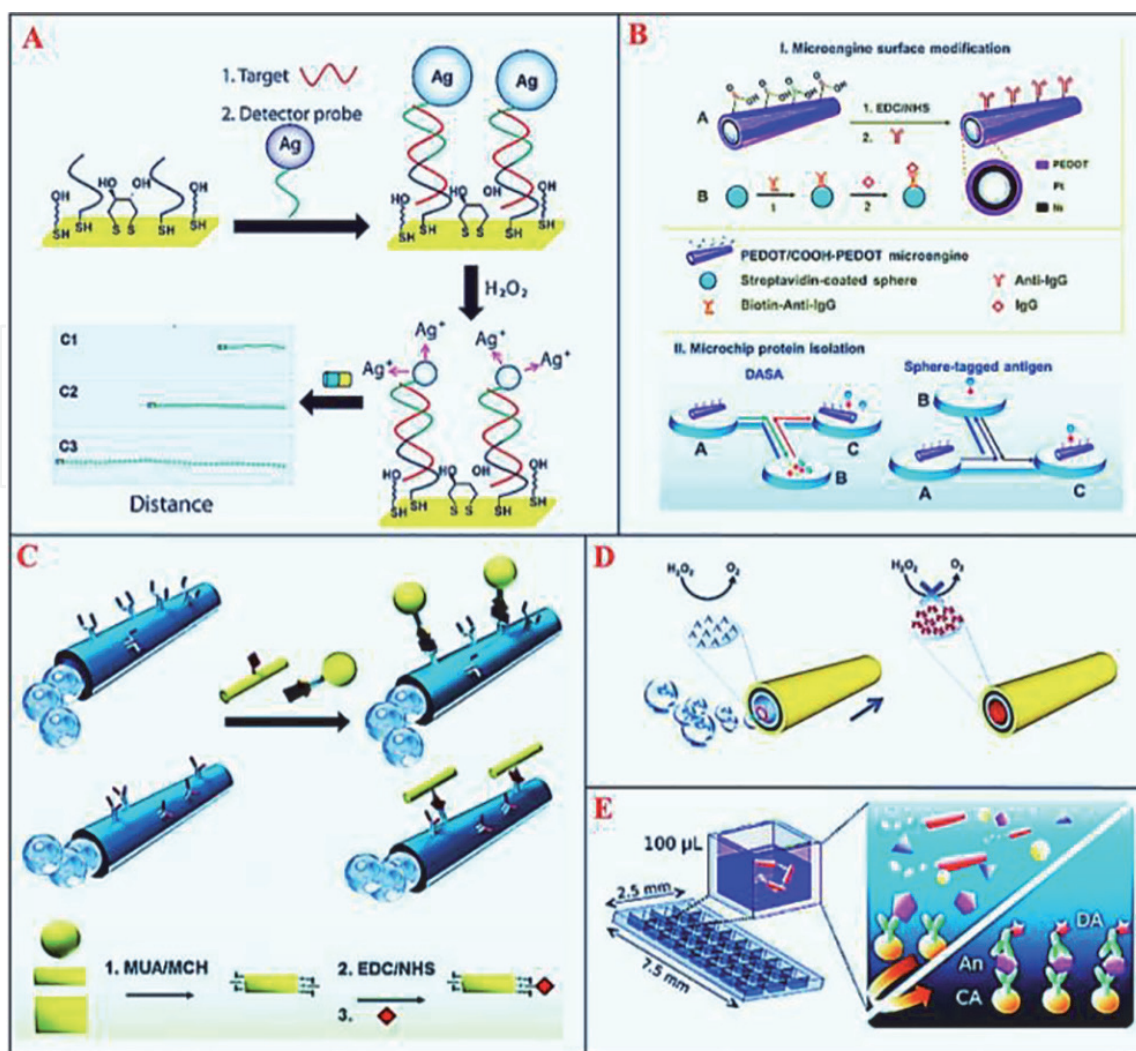


Figure 23. (A) Detection of Ag-tagged nucleic acid, which alters the propulsion of the micro-/nanomotors. (B) Antibody-decorated micromotor for protein detection. (C) Micromotor-based multiplexed immunoassay via different microscopic tracers. (D) Effect of the concentration of DMSO (dimethyl sulfoxide), cysteine, and serine on the swimming speeds of the microtubular motors. (E) Microarray immunoassay assisted by microengines. Copyright 2013, ACS Publications. Copyright 2012, ACS Publications. Copyright 2014, RSC Publications. Copyright 2013, RSC Publications. Copyright 2014, Wiley Online Library.

addition, the aforementioned vortex effect generated by the propulsion of micromotors can boost the mass transfer of the target toward the functionalized microjet surface (i.e. “on-the-fly”) as well as assist the mass transfer of the target molecule within the matrix of a sample solution toward a sensing surface, where the bio-receptor is situated and the target is expected to be selectively attached, as shown in **Figure 23E** [66].

5.4 Biomedical applications

The pioneering micro-/nanomotors offer considerable promise for biomedical applications, as shown in **Figure 24** [67]. Herein, we outline some important advances of micro-/nanomotors in the biomedical field.

Micro-/nanojets have proven to be capable of drilling into biomaterials and soft tissues. Rolled-up thin nanomembranes can asymmetrically result in sharp edges being engineered. Nanojets were self-propelled and externally directed toward immobilized cancer cells and embedded in their interior, as shown in **Figure 25A** [68]. However, the toxicity of the H_2O_2 fuel used for the movement leads to the cells undergoing apoptosis after short periods. Therefore, other environmentally

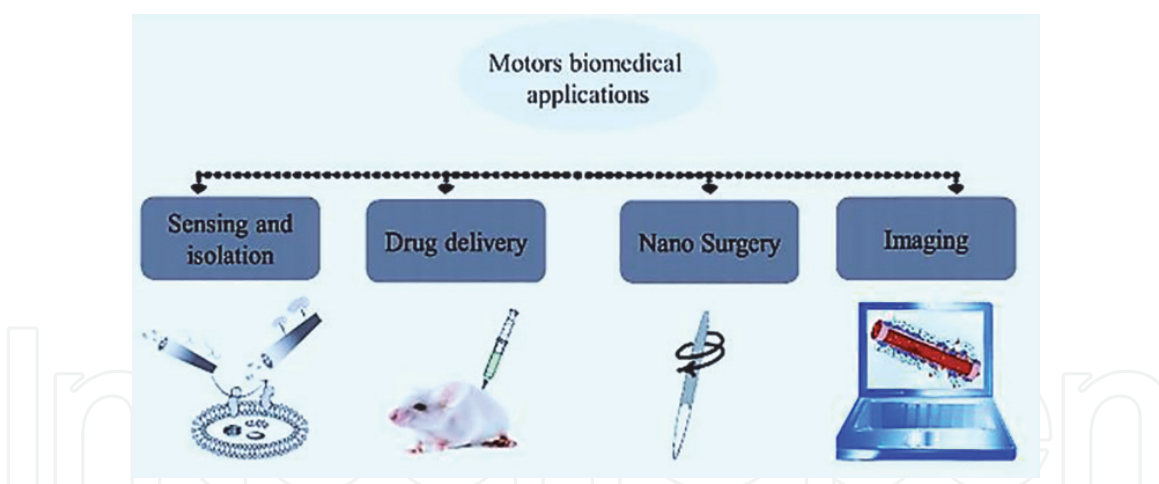


Figure 24.

Categories of biomedical applications of micro/nanomotors, including sensing and isolation, drug delivery, nanosurgery, biomedical imaging. Copyright 2014, RSC Publications.

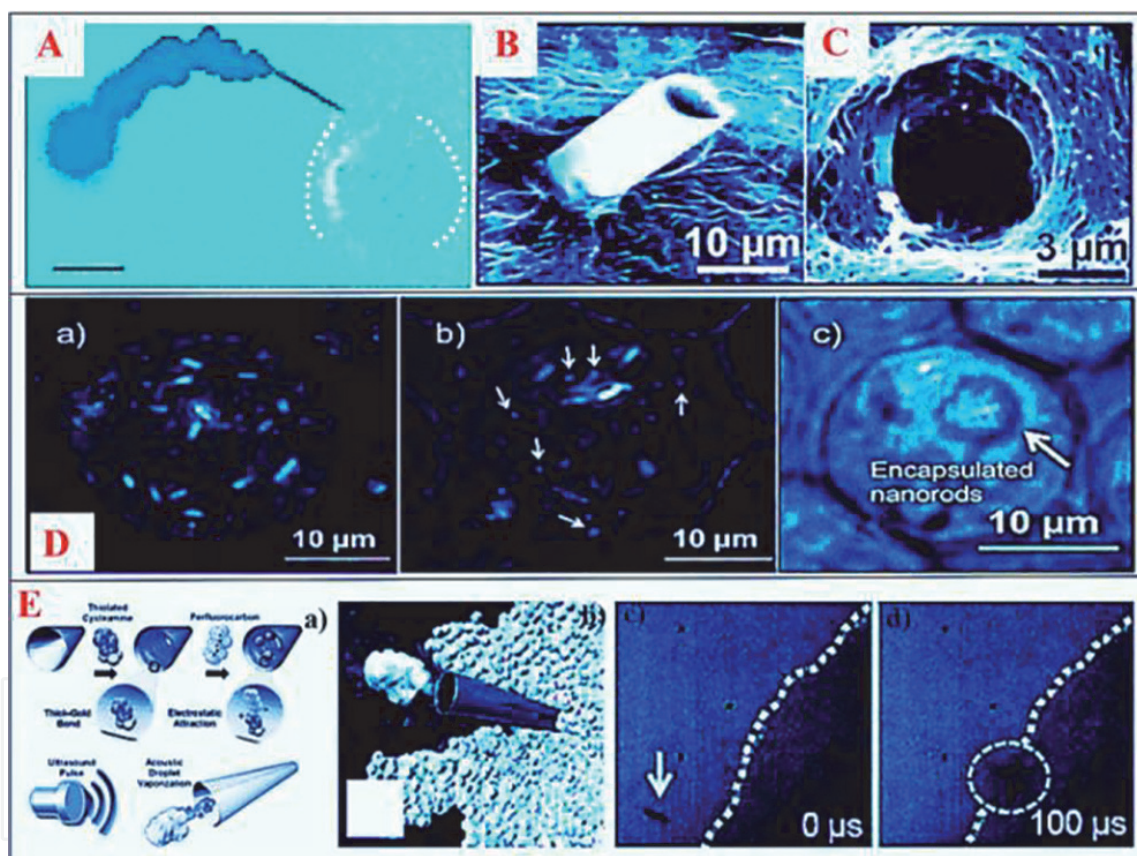


Figure 25.

(A) A catalytic nanojet drilling into an immobilized cancer cell. (B) SEM image of a magnetic microtube drilling into pig liver tissue. (C) Hole after removing the microtube. (D) Nanorods inside living HeLa cells: (a) multiple nanorods inside a HeLa cell, (b) subcellular structures (a few indicated by arrows) interacting with active acoustic motors inside a HeLa cell, and (c) two vesicular structures in a HeLa cell containing many active but crowded acoustic motors, respectively, can be seen. (E) Preparation and propulsion of perfluorocarbon-loaded microbullets (a), Computer-created diagram (b), and images of a microbullet penetrating a tissue after an ultrasound pulse (c and d), respectively. Copyright 2012, ACS Publications. Copyright 2013, RSC Publications. Copyright 2014, Wiley Online Library. Copyright 2012, Wiley Online Library.

friendly sources of movement are urgently required to replace H_2O_2 . Magnetic trigger can be used as an alternative to the motion. Conical microtubes powered by an external rotating magnetic field were placed onto liver tissue and drilled into it for long periods, as shown in **Figure 25B** [69]. After releasing the microtube from the biomaterial, a micrometer-sized hole was observed by SEM, as shown in

Figure 25C [69]. Ultrasonic waves can also generate the propulsion of micro-/nanomotors, as shown in **Figure 25D** and **E**) [70, 71]. Bio-functionalized nanowires propelled by ultrasound have been applied for bio-sensing, and the first results of magnetic steering toward cells have been studied. Mallouk et al. demonstrated the internalization of a nanowire-based motor inside living cells, as shown in **Figure 25D**. Developing biocompatible materials and fuels for artificial micro-/nanomotors or the use of noninvasive external triggered motors may pave the way for biomedical applications of micro-/nanomotors in the near future [72–80].

6. Conclusions

In this chapter, the previously reported Pt-based micro-/nanomotors are presented. In detail, the propulsion mechanisms, fabrication methods, propulsion controlling methods, and applications of these synthetic micro-/nanomotors developed in the past years are summarized accordingly. Despite the rapid and significant advances in micro-/nanomotors, challenges such as specifically practical applications and smart controlling still remain to be resolved. In addition, advanced structure design and fabrication methods are demanded.

Acknowledgements

This work was supported by Ministry of Education, Singapore, under “MOE 2011-T2-2-156, ARC 18/12” program.

Conflicts of interest

There are no conflicts of interest to declare.

Author details

Liangxing Hu^{1*}, Nan Wang² and Kai Tao³

1 Micromachines Lab, School of Mechanical and Aerospace Engineering, Nanyang Technological University, Singapore

2 Department of Science and Math, Singapore University of Technology and Design, Singapore

3 Ministry of Education Key Laboratory of Micro and Nano Systems for Aerospace, School of Mechanical Engineering, Northwestern Polytechnical University, Xi'an, China

*Address all correspondence to: lhu001@e.ntu.edu.sg

IntechOpen

© 2019 The Author(s). Licensee IntechOpen. This chapter is distributed under the terms of the Creative Commons Attribution License (<http://creativecommons.org/licenses/by/3.0>), which permits unrestricted use, distribution, and reproduction in any medium, provided the original work is properly cited. 

References

- [1] Stock D, Namba K, Lee LK. Nanorotors and self-assembling macromolecular machines: The torque ring of the bacterial flagellar motor. *Current Opinion in Biotechnology*. 2012;**23**:545
- [2] Schmidt JJ, Montemagno CD. Hybrid protein-polymer biomimetic membranes. *Annual Review of Materials Research*. 2004;**34**:315
- [3] Kinosita K, Yasuda R, Noji H, Adachi K. A rotary molecular motor that can work at near 100% efficiency. *Philosophical Transactions of the Royal Society B: Biological Sciences*. 2000;**355**:473
- [4] Wang J. Can man-made nanomachines compete with nature biomotors? *ACS Nano*. 2009;**3**:4
- [5] Wang W, Castro LA, Hoyos M, Mallouk TE. Autonomous motion of metallic microrods propelled by ultrasound. *ACS Nano*. 2012;**6**:6122
- [6] Wang Y, Hernandez RM, Bartlett DJ Jr, Bingham JM, Kline TR, Sen A, et al. Bipolar electrochemical mechanism for the propulsion of catalytic nanomotors in hydrogen peroxide solutions. *Langmuir*. 2006;**22**:10451
- [7] Wang J et al. Multi-fuel driven Janus micromotors. *Small*. 2013;**9**:467
- [8] Mirkovic T, Zacharia NS, Scholes GD, Ozin GA. Nanolocomotion-catalytic Nanomotors and nanorotors. *Small*. 2010;**6**:159
- [9] Patra D, Sengupta S, Duan W, Zhang H, Pavlick R, Sen A. Intelligent, self-powered, drug delivery systems. *Nanoscale*. 2013;**5**:1273
- [10] Whitesides GM et al. Autonomous movement and self-assembly. *Angewandte Chemie, International Edition*. 2002;**41**:652
- [11] Gibbs JG, Zhao YP. Design and characterization of rotational multicomponent catalytic nanomotors. *Small*. 2009;**5**:2304
- [12] Gibbs J, Zhao Y. Catalytic nanomotors: fabrication, mechanism, and applications. *Frontiers of Materials Science*. 2011;**5**:25
- [13] Paxton WF, Kistler KC, Olmeda CC, Mallouk TE, Sen A. Catalytic nanomotors: Autonomous movement of striped nanorods. *Journal of the American Chemical Society*. 2004;**126**:13424
- [14] Jiang HR, Yoshinaga N, Sano M. Active motion of a Janus particle by self-thermophoresis in a defocused laser beam. *Physical Review Letters*. 2010;**105**:268302
- [15] Baraban L, Streubel R, Makarov D, Han L, Karnaushenko D, Schmidt OG, et al. Catalytic Janus motors on microfluidic chip: deterministic motion for targeted cargo delivery. *ACS Nano*. 2012;**7**:1360
- [16] Mei YF, Solovev AA, Sanchez S, Schmidt OG. Rolled-up nanotech on polymers: From basic perception to self-propelled catalytic microengines. *Chemical Society Reviews*. 2011;**40**:2109
- [17] Gibbs JG, Zhao YP. Autonomously motile catalytic nanomotors by bubble propulsion. *Applied Physics Letters*. 2009;**94**(163103):1
- [18] Wang H, Pumera M. Fabrication of micro/nanoscalemotors. *Chemical Reviews*. 2015;**115**:8704
- [19] Demirok UK, Laocharoensuk R, Manesh KM, Wang J. Ultrafast catalytic alloy nanomotors. *Angewandte Chemie, International Edition*. 2008;**47**:9349

- [20] Laocharoensuk R, Burdick J, Wang J. Carbon-nanotube-induced acceleration of catalytic nanomotors. *ACS Nano*. 2008;**2**:1069
- [21] Gao W, Sattayasamitsathit S, Orozco J, Wang J. Highly efficient catalytic microengines: template electrosynthesis of polyaniline/platinum microtubes. *Journal of the American Chemical Society*. 2011;**133**:11862
- [22] Mirkovic T, Foo ML, Arsenault AC, Fournier-Bidoz S, Zacharia NS, Ozin GA. Hinged nanorods made using a chemical approach to flexible nanostructures. *Nature Nanotechnology*. 2007;**2**:565
- [23] Zhao G, Ambrosi A, Pumera M. Self-propelled nanojets via template electrodeposition. *Nanoscale*. 2013;**5**:1319
- [24] Gao W, Sattayasamitsathit S, Manesh KM, Weihs D, Wang J. Magnetically powered flexible metal nanowire motors. *Journal of the American Chemical Society*. 2010;**132**:14403
- [25] Wheat PM, Marine NA, Moran JL, Posner JD. Rapid fabrication of bimetallic spherical motors. *Langmuir*. 2010;**26**:13052
- [26] Valadares LF, Tao YG, Zacharia NS, Kitaev V, Galembeck F, Kapral R, et al. Catalytic nanomotors: self-propelled sphere dimers. *Small*. 2010;**6**:565
- [27] Gibbs JG, Fragnito NA, Zhao Y. Asymmetric Pt/Au coated catalytic micromotors fabricated by dynamic shadowing growth. *Applied Physics Letters*. 2010;**97**:253107
- [28] Lee TC, Alarcon-Correa M, Miksch C, Hahn K, Gibbs JG, Fischer P. Self-propelling nanomotors in the presence of strong Brownian forces. *Nano Letters*. 2014;**14**:2407
- [29] He Y, Wu J, Zhao Y. Designing catalytic nanomotors by dynamic shadowing growth. *Nano Letters*. 2007;**7**:1369
- [30] Huang W, Manjare M, Zhao Y. Catalytic nanoshell micromotors. *Journal of Physical Chemistry C*. 2013;**117**:21590
- [31] Solovev AA, Mei Y, Bermudez Urena E, Huang G, Schmidt OG. Catalytic microtubular jet engines self-propelled by accumulated gas bubbles. *Small*. 2009;**5**:1688
- [32] Solovev AA, Sanchez S, Pumera M, Mei YF, Schmidt OG. Magnetic control of tubular catalytic microbots for the transport, assembly, and delivery of micro-objects. *Advanced Functional Materials*. 2010;**20**:2430
- [33] Yao K, Manjare M, Barrett CA, Yang B, Salguero TT, Zhao Y. Nanostructured scrolls from graphene oxide for microjet engines. *Journal of Physical Chemistry Letters*. 2012;**3**:2204
- [34] Magdanz V, Stoychev G, Ionov L, Sanchez S, Schmidt OG. Stimuli-responsive microjets with reconfigurable shape. *Angewandte Chemie, International Edition*. 2014;**53**:2673
- [35] Li J, Zhang J, Gao W, Huang G, Di Z, Liu R, et al. Dry-released nanotubes and nanoengines by particle-assisted rolling. *Advanced Materials*. 2013;**25**:3715
- [36] Wu Y, Wu Z, Lin X, He Q, Li J. Autonomous movement of controllable assembled Janus capsule motors. *ACS Nano*. 2012;**6**:10910
- [37] Wilson DA, Nolte RJM, van Hest JCM. Autonomous movement of platinum-loaded stomatocytes. *Nature Chemistry*. 2012;**4**:268
- [38] Garcia-Gradilla V, Orozco J, Sattayasamitsathit S, Soto F, Kuralay F, Pourazary A, et al. Functionalized

ultrasound-propelled magnetically guided nanomotors: toward practical biomedical applications. *ACS Nano*. 2013;7:9232

[39] Wu Y, Lin X, Wu Z, Möhwald H, He Q. Self-propelled polymer multilayer Janus capsules for effective drug delivery and light-triggered release. *ACS Applied Materials & Interfaces*. 2014;6:10476

[40] Kline TR, Paxton WF, Mallouk TE, Sen A. Catalytic nanomotors: Remote-controlled autonomous movement of striped metallic nanorods. *Angewandte Chemie, International Edition*. 2005;44:744

[41] Zhao G, Pumera M. Magnetotactic artificial self-propelled nanojets. *Langmuir*. 2013;29:7411

[42] Baraban L, Makarov D, Streubel R, Mönch I, Grimm D, Sanchez S, et al. Catalytic Janus motors on microfluidic chip: deterministic motion for targeted cargo delivery. *ACS Nano*. 2012;6:3383

[43] Khalil ISM, Magdanz V, Sanchez S, Schmidt OG, Misra S. Three-dimensional closed-loop control of self-propelled microjets. *Applied Physics Letters*. 2013;103:172404

[44] Ahmed S, Wang W, Mair LO, Fraleigh RD, Li S, Castro LA, et al. Steering acoustically propelled nanowire motors toward cells in a biologically compatible environment using magnetic fields. *Langmuir*. 2013;29:16113

[45] Xu T, Soto F, Gao W, Garcia-Gradilla V, Li J, Zhang X, et al. Ultrasound-modulated bubble propulsion of chemically powered microengines. *Journal of the American Chemical Society*. 2014;136:8552

[46] Fan DL, Zhu FQ, Cammarata RC, Chien CL. Controllable high-speed rotation of nanowires. *Physical Review Letters*. 2005;94:247208

[47] Solovev AA, Smith EJ, Bufon CCB, Sanchez S, Schmidt OG. Light-controlled propulsion of catalytic microengines. *Angewandte Chemie, International Edition*. 2011;50:10875; *Angewandte Chemie*. 2011;123:11067

[48] Hong Y, Diaz M, Córdova-Figueroa UM, Sen A. Light-driven titanium dioxide based reversible microfireworks and micro-motor/micropump systems. *Advanced Functional Materials*. 2010;20:1568

[49] Sanchez S, Ananth AN, Fomin VM, Viehrig M, Schmidt OG. Superfast motion of catalytic microjet engines at physiological temperature. *Journal of the American Chemical Society*. 2011;133:14860

[50] Soler L, Martinez-Cisneros C, Swiersy A, Sanchez S, Schmidt OG. Thermal activation of catalytic microjets in blood samples using microfluidic chips. *Lab on a Chip*. 2013;13:4299

[51] Baraban L, Harazim SM, Sanchez S, Schmidt OG. Chemotactic behavior of catalytic motors in microfluidic channels. *Angewandte Chemie, International Edition*. 2013;52:5552; *Angewandte Chemie*. 2013;125:5662

[52] Sundararajan S, Lammert PE, Zudans AW, Crespi VH, Sen A. Catalytic motors for transport of colloidal cargo. *Nano Letters*. 2008;8:1271

[53] Sundararajan S, Sengupta S, Ibele ME, Sen A. Drop-off of colloidal cargo transported by catalytic Pt-Au nanomotors via photochemical stimuli. *Small*. 2010;6:1479

[54] Kagan D, Laocharoensuk R, Zimmerman M, Clawson C, Balasubramanian S, Kong D, et al. Rapid delivery of drug carriers propelled and navigated by catalytic nanoshuttles. *Small*. 2010;6:2741

- [55] Xuan M, Shao J, Lin X, Dai L, He Q. Self-propelled Janus mesoporous silica nanomotors with sub-100 nm diameters for drug encapsulation and delivery. *ChemPhysChem*. 2014;**15**:2255
- [56] Campuzano S, Kagan D, Orozco J, Wang J. Motion-driven sensing and biosensing using electrochemically propelled nanomotors. *Analyst*. 2011;**136**:4621
- [57] Campuzano S, Orozco J, Kagan D, Guix M, Gao W, Sattayasamitsathit S, et al. Bacterial isolation by lectin-modified microengines. *Nano Letters*. 2012;**12**:396
- [58] García M, Orozco J, Guix M, Gao W, Sattayasamitsathit S, Escarpa A, et al. Micromotor-based lab-on-chip immunoassays. *Nanoscale*. 2013;**5**:1325
- [59] Kuralay F, Sattayasamitsathit S, Gao W, Uygun A, Katzenberg A, Wang J. Self-propelled carbohydrate-sensitive microtransporters with built-in boronic acid recognition for isolating sugars and cells. *Journal of the American Chemical Society*. 2012;**134**:15217
- [60] Soler L, Magdanz V, Fomin VM, Sanchez S, Schmidt OG. Self-propelled micromotors for cleaning polluted water. *ACS Nano*. 2013;**7**:9611
- [61] Orozco J, Cheng GZ, Vilela D, Sattayasamitsathit S, Vazquez-Duhalt R, Valdes-Ramirez G, et al. Micromotor-based high-yielding fast oxidative detoxification of chemical threats. *Angewandte Chemie, International Edition*. 2013;**52**:13276; *Angewandte Chemie*. 2013;**125**:13518
- [62] Guix M, Orozco J, Garcia M, Gao W, Sattayasamitsathit S, Merkoci A, et al. Superhydrophobic alkanethiol-coated microsubmarines for effective removal of oil. *ACS Nano*. 2012;**6**:4445
- [63] Campbell AI, Ebbens SJ. Gravitaxis in spherical Janus swimming devices. *Langmuir*. 2013;**29**:14066
- [64] Vilela D, Orozco J, Cheng G, Sattayasamitsathit S, Galarnyk M, Kan C, et al. Multiplexed immunoassay based on micromotors and microscale tags. *Lab on a Chip*. 2014;**14**:3505
- [65] Zhao GJ, Sanchez S, Schmidt OG, Pumera M. Poisoning of bubble propelled catalytic micromotors: the chemical environment matters. *Nanoscale*. 2013;**5**:2909
- [66] Morales-Narváez E, Guix M, Medina-Sánchez M, Mayorga-Martinez CC, Merkoçi A. Micromotor enhanced microarray technology for protein detection. *Small*. 2014;**10**:2542
- [67] Loai KEA, Abdelmohsen F, Peng YFT, Wilson DA. Micro- and nano-motors for biomedical applications. *Journal of Materials Chemistry B*. 2014;**2**:2395
- [68] Solovev AA, Xi W, Gracias DH, Harazim SM, Deneke C, Sanchez S, et al. Self-propelled nanotools. *ACS Nano*. 2012;**6**:1751
- [69] Xi W, Solovev AA, Ananth AN, Gracias DH, Sanchez S, Schmidt OG. Rolled-up magnetic microdrillers: towards remotely controlled minimally invasive surgery. *Nanoscale*. 2013;**5**:1294
- [70] Wang W, Li SX, Mair L, Ahmed S, Huang TJ, Mallouk TE. Acoustic propulsion of nanorod motors inside living cells. *Angewandte Chemie, International Edition*. 2014;**53**:3201; *Angewandte Chemie*. 2014;**126**:3265
- [71] Kagan D, Benchimol MJ, Claussen JC, Chuluun-Erdene E, Esener S, Wang J. Acoustic droplet vaporization and propulsion of perfluorocarbon-loaded microbullets for targeted tissue penetration and deformation. *Angewandte Chemie, International Edition*. 2012;**51**:7519; *Angewandte Chemie*. 2012;**124**:7637

- [72] Hu LX, Miao JM, Grüber G. Disk-like nanojets with steerable trajectory using platinum nozzle nanoengines. *RSC Advances*. 2016;**6**:3399
- [73] Hu LX, Miao JM, Grüber G. Temperature effects on disk-like gold-nickel-platinum nanoswimmer's propulsion fuelled by hydrogen peroxide. *Sensors and Actuators, B: Chemical*. 2017;**239**:586
- [74] Hu LX, Tao K, Miao JM, Grüber G. Hydrogen-peroxide-fuelled platinum-nickel-SU-8 microrocket with steerable propulsion using an eccentric nanoengine. *RSC Advances*. 2016;**6**:102513
- [75] Hu LX, Wang N, Miao JM, Grüber G. Investigation of temperature dependency on the propulsion of disk-like nanoswimmers. *Procedia Technology*. 2017;**6**:48
- [76] Hu LX, Rehman S, Tao K, Miao JM. Characterization on three-dimensional trajectory of disk-like gold-nickel-platinum nanomotor using digital holographic imaging. *ChemistrySelect*. 2018;**3**:9634
- [77] Hu LX, Tao K, Lim YD, Miao JM, Kim YJ. Self-steerable propulsion of disk-like micro-craft with dual off-center nanoengines. *ACS Applied Energy Materials*. 2019;**2**:1657
- [78] Wang N, Kanhere E, Tao K, Hu LX, Wu J, Miao JM, et al. Investigation of a thin-film quasi-reference electrode fabricated by combined sputtering-evaporation approach. *Electroanalysis*. 2019;**31**:560
- [79] Astorga SE, Hu LX, Marsili E, Huang YZ. Ordered micropillar array gold electrode increases electrochemical signature of early biofilm attachment. *Materials & Design*. 2020;**185**:108256
- [80] Tao K, Yi HP, Yang Y, Chang HL, Wu J, Tang LH, et al. Origami-inspired electret-based triboelectric generator for biomechanical and ocean wave energy harvesting. *Nano Energy*. 2020;**67**:104197